Room temperature synthesis of gold nanoparticles in microchannel reactor

A Project Report
submitted in partial fulfillment of the
requirements for the degree of
Master of Engineering
in the Faculty of Engineering
by

Parveen

Department of Chemical Engineering
Indian Institute of Science
Bangalore 560 012 (India)

June 2010

Contents

List of Figures

List of Tables

Abstract

Nanoparticles are one of the fundamental building blocks of nanotechnology. Nanoparticles are used in a variety of fields like health care, electronics, biology, catalysis, all of which require monodisperse nanoparticles as physico-chemical properties like melting point, chemical reactivity change dramatically with particle size. As such their controlled synthesis is an important research and development challenge. Nanoparticles are synthesized by two techniques; gas and liquid phase techniques. Liquid phase technique provides better control over the polydispersity of nanoparticles as compared to gas phase synthesis. For continuous synthesis in liquid phase, microchannel reactors are typically used. Currently, scaling up of microchannel reactors is hindered due to fouling as it results in heterogeneous nucleation, thereby affecting the particle size. The objective of the present work is to study the effects of different engineering aspects on nanoparticle synthesis in microchannel reactors. This report begins with a brief literature review on nanoparticle synthesis in microchannel reactor. In the next part various designed developed to control size dispersion in microchannel reactors are discussed. In the final part of the report experimental results are discussed.

Chapter 1

Introduction

Objective

Nanoparticles are defined as particles having diameter less than 100 nm (Kruis *et al.*, 1998). Nanoparticles have application in many industries like electronics(José-Yacamán *et al.*, 1998), photonic (Haus *et al.*, 1993), chemical (Hepel, 1998), ceramics (Schmid *et al.*, 1998), metallurgical(José-Yacamán *et al.*, 1998), pharmaceutical (Allémann *et al.*, 1998) etc. Most of these applications are based upon the size and shape dependent properties of nanoparticles and require highly monodisperse particles, which have coefficient of variance (C.V.) $< 5\%$.

There are two approaches towards synthesis of nanoparticles: "top down" and "bottom up". In top down approach, large size particles are broken into smaller sizes using techniques like crushing, grinding, attrition. These methods are highly energy inefficient and lead to poor control over the size distribution. In bottom up approach, nanoparticles are synthesized from molecules (Mijatovic *et al.*, 2005). This can be further classified into gas phase synthesis and liquid phase synthesis. Gas phase synthesis are high temperature processes that can produce large particles in large quantity but require sophisticated equipments which are difficult to control(Gutsch *et al.*, 2002). In liquid phase synthesis, redox precursors are mixed under different operating condition to produce

nanoparticles.

Presently, with batch protocols ((Turkevich *et al.*, 1951), (Brust *et al.*, 1994), (Slot and Geuze, 1985)) nanoparticles of desired size and shape can be synthesized but scaling up requires overcoming issues like temperature control, concentration gradient etc (Mantzaris, 2005). Microchannel reactors, used for continuous synthesis, are basically three dimensional structures having one of the dimensions in sub-millimeter scale. These reactors have high surface to volume ratio and high heat transfer coefficient than conventional reactors. Also mixing and diffusion time scales are very small, so, effect of mass transfer on chemical reactions is negligible(Jähnisch *et al.*, 2004). A problem with these reactors is that nanoparticles deposit on the wall which causes heterogeneous nucleation and affects the particle size being formed. Thus, formation of monodisperse particles remain a challenge in microchannel reactor(Wagner and Köhler, 2005). This report begins with a brief literature review on nanoparticle synthesis in microchannel reactor. In the next part different attempts made in our lab to control size dispersion in microchannel reactors are discussed. In the final part of the report experimental results are discussed.

Chapter 2

Literature survey

Gold nanoparticles have emerged as one of the building blocks of nanotechnology because of the diversity in their applications. They have found applications in areas like biology (Daniel and Astruc, 2004), electrochemistry (Guo and Wang, 2007), catalysis ((Haruta, 2002), (Tsunoyama *et al.*, 2008)), electronics (Shipway *et al.*, 2000) etc.

2.1 Standard protocols of gold nanoparticle synthesis

In liquid phase synthesis, gold particles are synthesized by reduction of gold salt using a reducing agent. Commonly employed protocols for synthesizing gold nanoparticles are those developed by Turkevich *et al.* (1951), Slot and Geuze (1985) and Brust *et al.* (1994).

Turkevich *et al.* (1951) synthesized gold nanoparticles by reducing chloroauric acid with sodium citrate at 100 ^{0}C. This method is widely known as the 'Citrate method'. Reaction time is typically 5 minutes and it increases with a decrease in temperature. The mean diameter of the nanoparticles is typically 20 nm $\pm$ 1.5 nm with a C. V. 12.5%. The mean particle size decreases with an increase in the molar ratio of sodium citrate to chloroauric acid. Slot and Geuze (1985) synthesized gold nanoparticles using a mixture of sodium citrate and tannic acid as the reducing agent at 60 ^{0}C. Particle size and reaction time both depend

on the amount of tannic acid present in the reducing solution. Reaction time changes from one hour to few seconds as the amount of tannic acid varies from zero to maximum (5 ml of 1% tannic acid solution). So it can be concluded that the kinetics of gold salt reduction by tannic acid is faster when compared to that of sodium citrate. Average particle diameter varies from 17 nm to 3 nm with variation in amount of tannic acid from 10 μL to 5 mL (1% tannic acid solution). Solutions formed are nearly monodisperse with C. V. values $< 10\%$. Brust *et al.* (1994) reduced the gold salt solution in a two-phase solution (water-toluene) using tetraoctyl ammonium bromide as a phase transfer agent. Dodecanethiol is used as the caping agent. Thiol coated particles having diameter from 1 to 3 nm are formed in the organic phase (toluene). Particles formed by the Brust protocol are much smaller in size as compared to the two methods described earlier.

2.2 Synthesis of gold nanoparticle synthesis in microchannel reactor

Wagner *et al.* (2004) reported seeded growth approach for making gold nanoparticles using ascorbic acid as reducing agent and polyvinylpyrrolidone (PVP) as stabilizing agent in a microchannel reactor which is wet etched in Pyrex glass and covered with a layer of silicon that is anodically bonded to the glass. In this method gold nanoparticles with a mean diameter of 11.7 $\pm$ 0.9 nm are used as seeds. These seeds were synthesized by 'Citrate Method'(Turkevich *et al.*, 1951). Particle size increases significantly in all the experiments conducted (mean diameter 15 to 24 nm). Particles formed with PVP are more stable. Particles having diameter up to 12 nm could be handled without clogging of channel. Köhler *et al.* (2005) have synthesized gold nanoparticles in microchannnel reactor based upon the design of Kirner *et al.* (2004). Reactor has three mixing zones and each mixing zone has splitting, reshaping and recombination units. Syringe Pumps

are used for pumping reactant solutions. Ascorbic acid and Ferrous sulphate are used as the reducing agent. Sodium meta silicate and poly vinyl alcohol are used as the stabilizing agents. Citrate is used as a buffering agent. Change in flow rate ratios of different reactants results in different size distribution of gold nanoparticles (5 nm at equal flow rate of all reactants 1 μL/min; large particles at 25 μL/min of ascorbic acid, 25 μL/min of poly vinyl alcohol, 25 μL/min of cholroauric acid, 5 μL/min of sodium meta silicate; aggregate particles at 25 μL/min of ascorbic acid, 5 μL/min of poly vinyl alcohol, 25 μL/min of chloroauric acid, 2 μL/min of sodium meta silicate). Wagner and Köhler (2005) performed the synthesis of gold nanoparticles in a continuous flow microreactor designed by Kirner *et al.* (2004) using ascorbic acid as the reducing agent. PVP is added to the chloroauric solution as the stabilizing agent. Design of the reactor is such that flow direction changed from horizontal to vertical and vice versa at reunification and branching points to get efficient inter diffusion. Deposition of particles on the wall was minimized by altering the chemical properties of internal surface of the channel by any of the following two methods:

1. Maintaining the solution at pH 9.5 which makes the glass surface negatively charged by reducing Si-OH to SiO^-. The electrostatic repulsion between surface and negatively charged gold particles suppresses the deposition of gold nanoparticles.

2. Making the internal surface hydrophobic via silanization with trichloro-perfluoro- octyl silane.

Mean particle size also decreases with increase in flow rate (35 nm at 100 μL/min. to 24 nm at 800 μL/min.), which is attributed to higher nucleation rate at higher flow rate. They found that the concentration of gold particles increases with an increase in flow rate, and that at higher flow rates deposition was higher, which was attributed to higher shear stresses. An increase in ratio of ascorbic

acid to gold salt solution decreases the particle size which is attributed to the fact that the higher concentration of reducing agent results in higher number of nuclei formed and a shorter growth phase. Also mean diameter of the particles decrease with increase in pH (21 nm at pH 2.8 to 2.9 nm at pH 9.5);because at higher pH, electrostatic repulsion avoids the deposition of the particles at the wall. Shalom *et al.* (2007) synthesized thiol coated gold nanoparticles using 'Brust method' in microchannel reactor design comprising of a radial interdigitated mixer. Channel surface is silanised using trichloro-perfluoro-octyl silane. Particles synthesized in microchannel are considerably smaller in size and have lower polydispersity as compared to particles synthesized in batch mode. Furthermore, smaller size particles are obtained with increase in flow rate as residence time becomes smaller. Tsunoyama *et al.* (2008) synthesized gold nanoparticles in a microchannel reactor by reducing chloroauric acid with sodium borohydride, and using PVP as a stablizing agent. Microchannel is made up of Hastelloy and has a counterflow configuration consisting of 32 channels. The outlet is single channel having inner diameter 0.5 mm. PVP stabilized monodisperse particles of size approximately 1 nm were synthesized. Particles are smaller in size as compare to particles synthesized in batch system. The particles synthesized were also used as catalyst for aerobic oxidation of p-hydroxybenzyl alcohol to p-hydroxybenzaldehyde.

Chapter 3

Initial work [performed by Inyan, 2009]

Preliminary experiments on utilizing an in-house developed, room temperature, rapid protocol (Sankar *et al.*, Manuscript under review, 2010) were carried out by Iniyan (2009). These experiments were done with a Y shaped PDMS microchannel reactor, which was designed in-house. Initially oscillations were observed at the Y junction of the reactor. This was attributed to the continual stop-start motion of the stepper motor used to drive syringe pumps. To dampen these oscillations, PDMS reservoirs (figure 3.1) were deployed to act as capacitor between the syringe and inlet tube.

Figure 3.1: Digital micrograph of PDMS reservoir

Gold nanoparticles were synthesized following the protocol of Sankar *et al.* (Manuscript under review, 2010). 0.57 mM gold chloride solution was injected at the rate of 2x10^{-9} m^3/s through one arm of the Y-channel and 0.87 mM tannic acid solution flowing at the rate of 2x10^{-9} m^3/s was run through another arm. One of the major issues with this set-up is the deposition of gold nanoparticle on the wall of the reactor. This resulted in heterogeneous nucleation, leading to polydisperse particles. It was observed that deposition occurred mainly on the side of gold solution in the channel (figure 3.2). This was attributed to the acidic pH present on chloroauric acid side which weakens the stabilization.

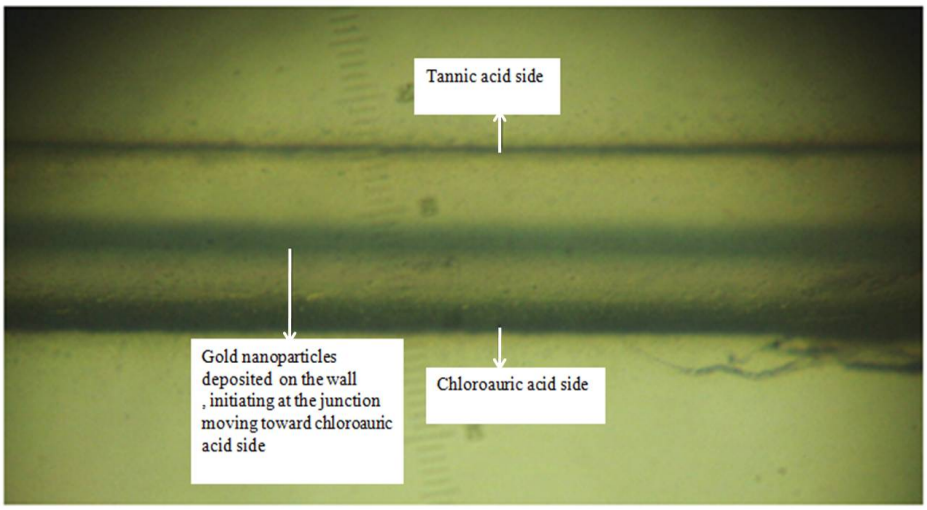

Figure 3.2: Digital micrograph highlighting the deposition of gold nanoparticles in Y-shape microchannel reactor

A reactor with concentric coaxial geometry (core flow) was designed to overcome the problem of particle deposition on the wall. In the core flow, gold salt solution ($HAuCl_4$) flows in the center (inner diameter = 360 μm) while reducing/stablizing agent (tannic acid) flows in the outer region surrounding the gold salt solution. This geometry avoids contact between reaction interface and the walls of the channel, however the design of inlet pathways becomes more in-

volved. A core flow microchannel reactor with PDMS inlets was designed in two steps (Appendix A).

The TEM micrographs showed the presence of highly polydisperse particles, in contrast to bulk protocol (figures $A.4$, $A.5$, $A.6$, $A.7$ of Appendix A). A careful analysis indicated that gold particles are formed at the interface, after which particles can diffuse either into chloroauric acid solution or tannic acid, which provide different stylizing environment. Particles in gold solution will be larger in size as compared to particles in tannic acid solution, resulting in polydispersity. This also reveals that the redox reaction is much faster than the time required for diffusion of tannic acid into the core followed by adsorption and stabilization of gold nanoparticles.

To overcome this issue we decided to design, a microchannel reactor with 'core in core' flow. In 'core in core' microchannel reactor, gold salt solution flows in between two layers of the reducing agent (figure 3.3) and the design is such that the effective separation length scale is of the order of 10's of microns.

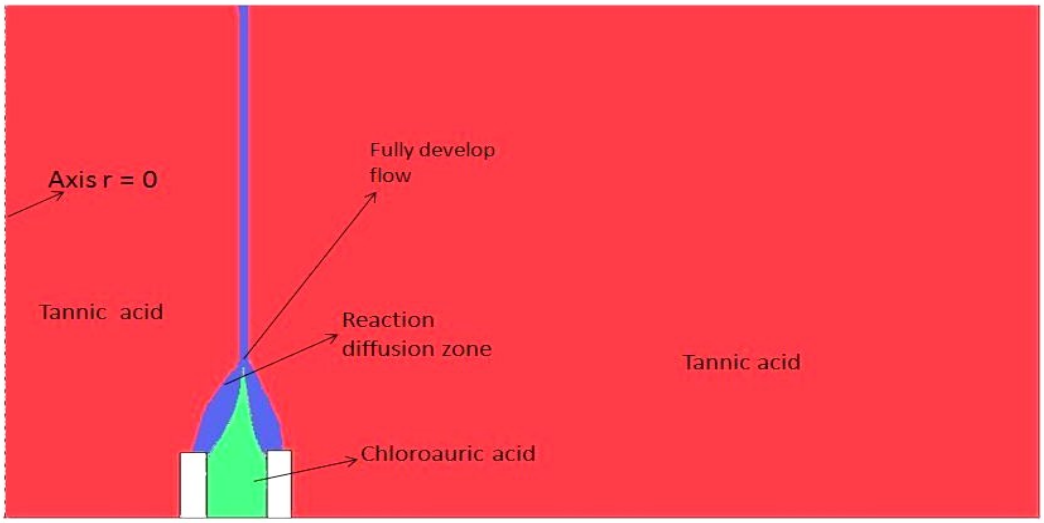

Figure 3.3: Schematic representation of the proposed 'core in core' flow microchannel reactor

The blue colour regions depict the expected diffuse reaction zone in which nanoparticles are formed. The desired interface evolution is also depicted. The idea is to have minimal interfacial area between diffuse reaction zone and chloroauric acid solution. This can avoid coagulation of nuclei/particles that leads to polydispersity.

Chapter 4

Microchannel reactor designs developed in this work

4.1 Materials used for fabrication of microchannel reactor

Polydimethylsiloxane (PDMS), a silicon based organic polymer, is commonly used for making microchannel reactors. It is inert, nontoxic, non-flammable and optically clear. Its chemical formula is $(H_3C)_3SiO[Si(CH_3)_2O]_nSiCH_3$, where n is the number of monomer units. It has hydrophobic surface which makes PDMS structures compatible with polar solvents (such as water, alcohol) without deformation. On the other hand, organic solvents will diffuse into the material and swell it, making them incompatible with PDMS devices (Rolland *et al.*, 2004). Brust *et al.* (1994) showed that particles synthesized in organic phase are much smaller in size in comparison with the particles synthesized in aqueous phase synthesis. Thus, glasses and other materials (e.g. SU-8) which are compatible with both aqueous and organic medium are also used for the fabrication of microchannel reactors.

4.2 'Core in core' flow microchannel reactor

As glass is compatible with both aqueous and organic phase reactions, 'core in core' flow microchannel was fabricated of the same with the help of glass blowing facility at IISc (figure 4.1). Dimensions of 'core in core' flow microchannel reactor are given in table 4.1. The length of the channel was 29 cm.

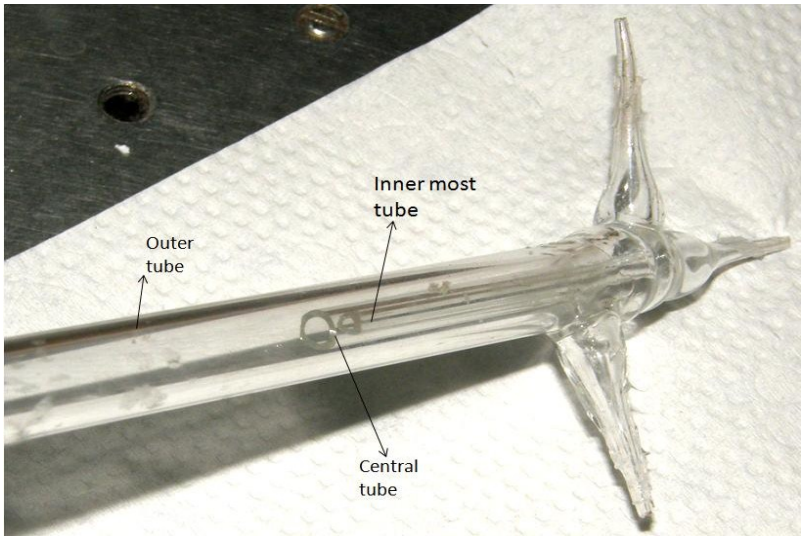

Figure 4.1: Digital micrograph of 'core in core' flow microchannel reactor

Table 4.1: Dimensions of 'core in core' flow microchannel reactor

Tube	Inner diameter (mm)	Outer diameter (mm)
Inner most tube	1.3	2.5
Central tube	3.0	4.3
Outer most tube	7.0	10.0

Inlet connections to the channel were provided using PTFE tubes by heating the glass inlets at the gas burner and then fitting PTFE tubes over them. To avoid leakage silicone sealant was used. After applying silicone sealant, whole setup was heated in the oven at 60 ^{0}C for 20 minutes (figure 4.2).

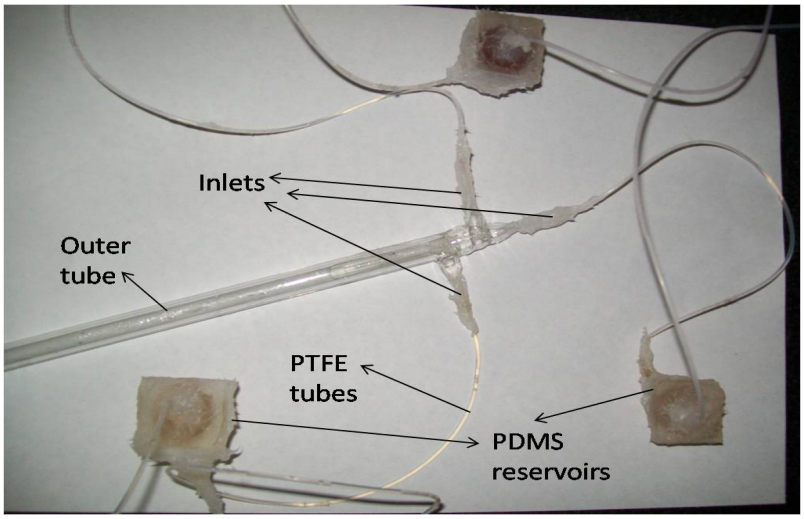

Figure 4.2: Digital micrograph showing inlet connections to 'core in core' flow microchannel reactor

Initial experiments were carried out with dye and deionized water to study the flow patterns in the channel. Dye was injected into the annular region with a flow rate of 0.02 mL/s and water was passed in the innermost and outer channels with flow rates of 0.02 mL/s and 0.2 mL/s respectively. The optimum of flow rates ratios to be used in different regions were found by simulating Navier-Stokes equation using COMSOL Multiphysics software as discussed in chapter 5.

The following precautions were used to guide the experiments implementation.

1. Flow rates in three regions chosen so that the velocities should be of the same order to avoid secondary circulation.

2. While filling the liquid in one inlet, other two inlets should be kept closed to avoid back flow.

3. During cleaning of channel with aquaregia, all the inlets should be kept closed to avoid excessive back flow into the sealant covered joints.

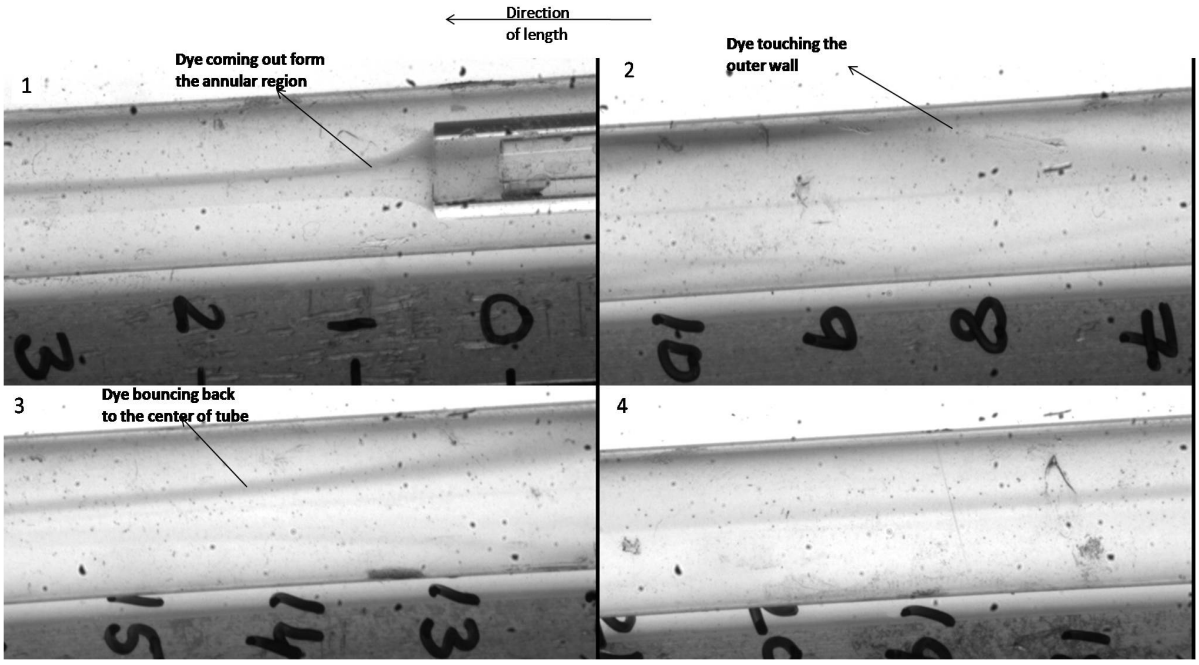

Figure 4.3: Snapshots of dye experiment performed in 'core in core' flow microchannel reactor

Figure 4.3 shows the snapshots of dye experiment performed in 'core in core' flow microchannel reactor. Flow pattern in the 'core in core' flow microchannel reactor shows that dye was touching the wall and bouncing back. This flow pattern can be attributed to swirling instabilities leading, which have been observed in other situations (Dyke, 1988). This could not be avoided in fabricated channel, so this was not pursued further as it leads to uncontrollable flow patterns.

4.3 core flow microchannel reactors with 50 and 100 micron core diameters

The idea of 'core in core' flow microchannel reactor is to have a thin gold salt solution layer so that particles formed at interface diffuse mostly in tannic acid, leading to low polydispersity. This can also be achieved from core flow microchannel reactor with very small size core. So, Core flow microchannel reactors with 50

micron core diameter and 100 micron diameters were fabricated (after procuring such thin capillary tubing).

4.3.1 Fabrication of microchannel reactor with 50 micron core diameter

1. A glass tube of inner diameter approximately 2.5 mm and outer diameter approximately 5.5 mm with side entry was fabricated using glass blowing facility at IISc.

2. A PEEK tube of inner diameter 50 micron and outer diameter 360 micron was fitted in a micropipette.

3. Now PDMS base and curing agent were taken in the ratio 10:1 by weight in a petridish. Base and curing agent were mixed thoroughly by stirring the mixture manually for 15 minutes. Then the petridish containing PDMS was put in a vacuum desiccator for 5 minutes to remove air bubbles.

4. PDMS was poured into the micropipette tip and heated in an oven for 30 minutes at 60 ^{0}C.

5. The micropipette tip is then fitted on the end of glass while ensuring that micropipette tip is in the center of tube. Silicone sealant was applied to avoid leakage. Araldite is applied over silicone sealant to strengthen the joint.

6. To make inlet connection to outer region, PTFE tube was used while inlet connection to core side was made using TEE interconnect (LabSmith, 360 μm single user kit). TEE connector has three openings. One is blocked using One-piece plug (LabSmith, 360 μm single user kit). Other two sides are connected to syringe and 50 micron capillary using One piece fittings (LabSmith, 360 μm single user kit) respectively (figure 4.4).

7. To supply fluids syringe pumps were used. For core side supply, special syringe was designed. Syringe was fitted with One piece fitting (LabSmith) using a micropipette tip. Araldite was applied at the joints to avoid leakage (figure 4.5).

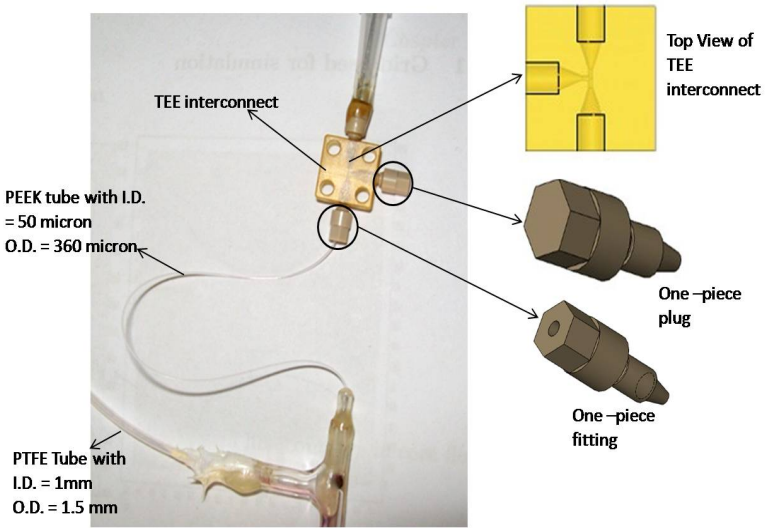

Figure 4.4: Digital micrograph of core flow microchannel reactor having core diameter 50 micron

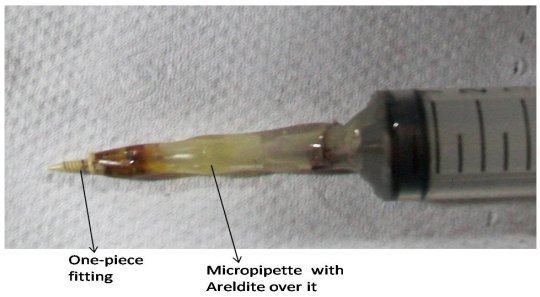

Figure 4.5: Digital micrograph of syringe used for supplying liquid in core side

Core flow microchannel reactor with core diameter 100 micron was fabricated in same way as 50 micron core flow microchannel reactor was done.

Initial experiments were carried out with dye and deionized water to study the flow pattern in the 50 micron core flow microchannel reactor. Dye flowed in the center at a flow rate of 0.01 mL/s and water flowed in the outer region at a flow rate of 0.1 mL/s. This flow rate ratio was validated theoretically by simulating Navier-Stokes equation which is discussed in chapter 5.

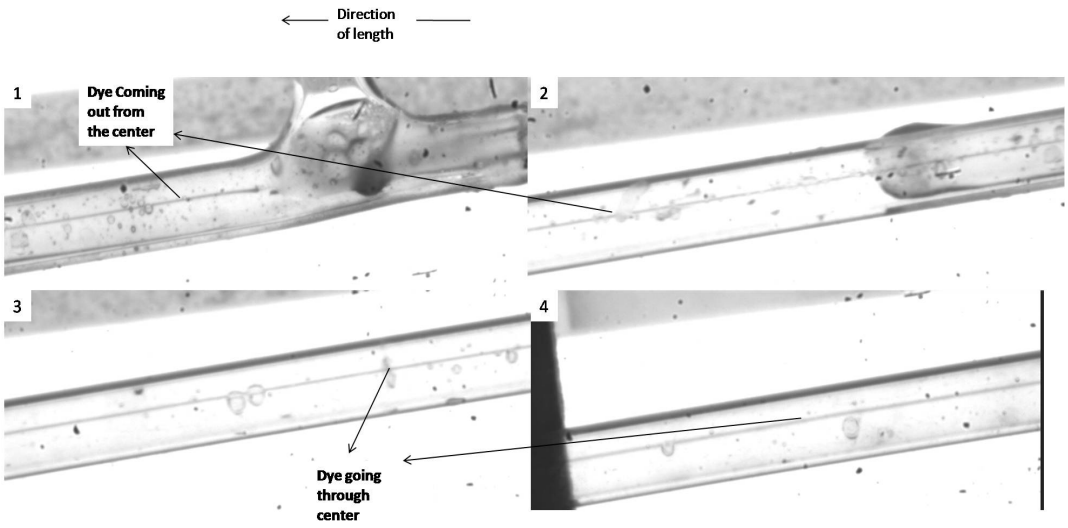

Figure 4.6: Snapshots of dye experiment conducted in 50 micron core microchannel reactor

Figure 4.6 shows snapshots of the dye experiment performed in 50 micron core flow microchannel reactor. This indicates that the desired flow pattern was maintained in the channel.

Chapter 5

Flow simulations of microchannel reactors

As the reaction between tannic acid and gold salt solution is very fast, the length and time scales over which flow become fully developed are of importance to understand the possible effects of transition flow on nanoparticle size distribution. To estimate these lengths and time scales, we carried out simulation of Navier-Stokes equation for desired geometry using COMSOL Multiphysics software. COMSOL Multiphysics is software based upon finite element analysis which is used for solving various physics and engineering problems. To validate our implementation of COMSOL Multiphysics software, we simulated a core flow microchannel geometry reported in literature by Andreev *et al.* (1999). They modelled the coaxial jet mixer having similar geometry and dimensions (figure 5.1) as of core flow microchannel reactor and solved the Navier-Stokes equation and diffusion-convection equation using finite volume method for two values of the Reynolds number (10.9 and 32.7).

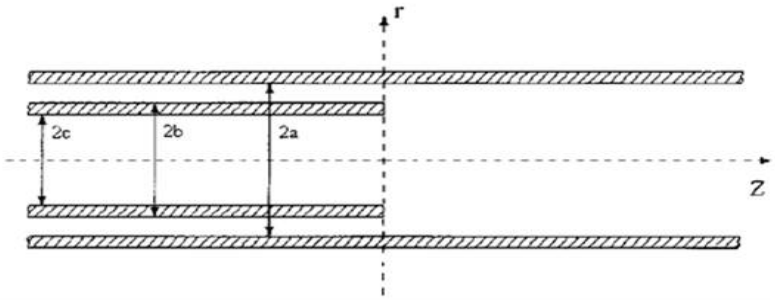

Figure 5.1: Cross-section of coaxial jet mixer, where 2a= 580 μm, 2b= 350μm and 2c= 247 μm

In the present study COMSOL Multiphysics was used to solve Navier-Stokes equation for the same geometry for Reynolds number 10.9. Traingular grid was used for the simulation as shown in figure $A.8$ of Appendix A. A comparison of stream line contours for three different ratios of inner to outer flow rates with those given by Andreev *et al.* (1999) is presented in figure 5.2. The comparison shows the similar kind of flow patterns, validating our implementation of the COMSOL platform. Navier-Stokes equation was then simulated for 'core in core' flow microchannel reactor and 50 micron core flow microchannel reactor.

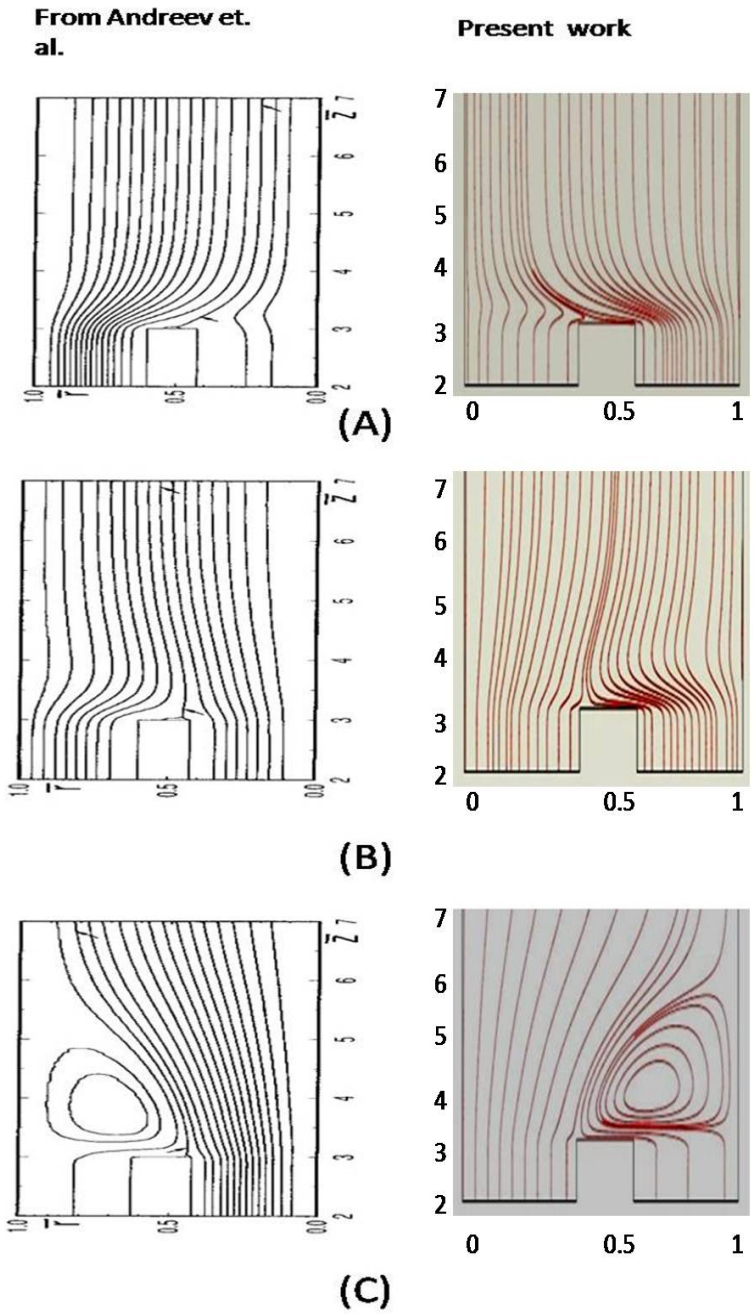

Figure 5.2: Comparison of stream line contours for the three different values of the ratio of inner to outer flow rate ((A)=Q$_{in}$: $Q_{out} = 1 : 11, (B) = Q_{in} : Q_{out} = 1 : 1, (C) = Q_{in} : Q_{out} = 11 : 1$)

5.1 Simulation of Navier-Stokes equation for 'core in core' flow microchannel reactor

Simulation of Navier-Stokes equation for 'core in core' geometry was carried out to estimate the ratio of operating flow rates in different regions (figure 5.3, figure 5.4), so that steady laminar flow is achieved at the earliest. The grid used for simulation is shown in figure A.9 of appendix A.

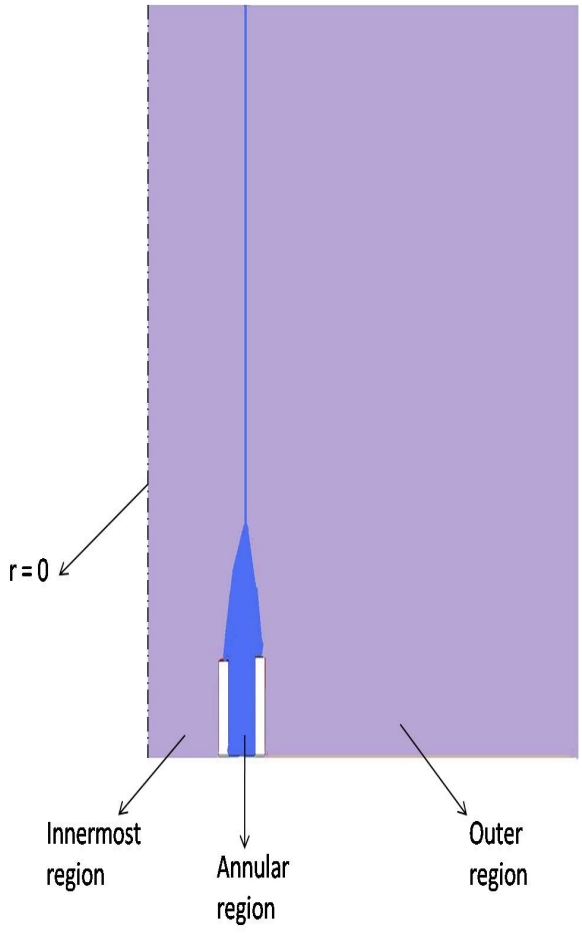

Figure 5.3: Schematic diagram of 'core in core' flow microchannel reactor

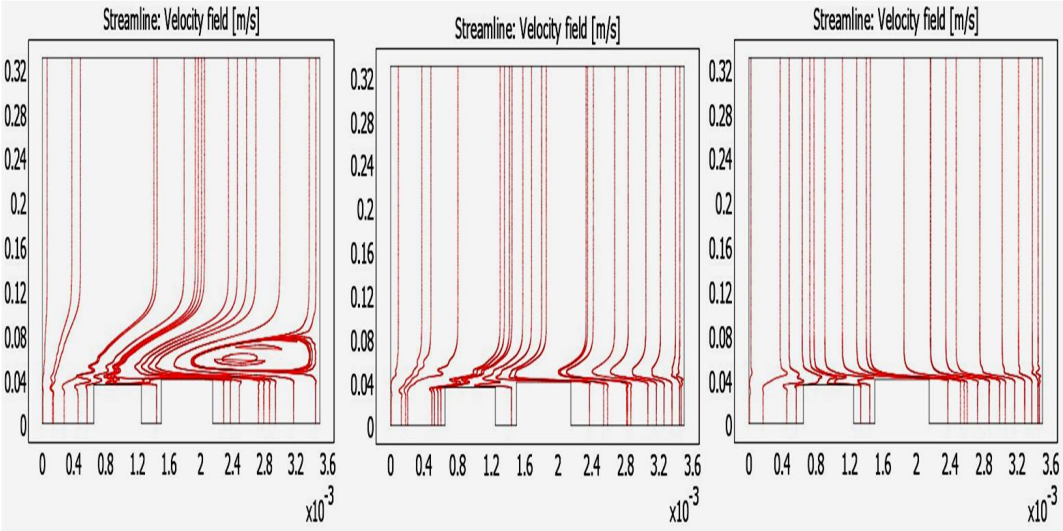

Figure 5.4: Stream line contours for three different flow rate ratios inner to annular to outer region (12.6:1:12.6, 6.25:1:12.6, 1:1:12.6)

when innermost region flow rate was higher, a vortex is formed near the inlet which causes undesirable mixing. In the successive simulations innermost flow rate was decreased so that vortex formation can be avoided. The best ratio was found to be 1:1:12.6 and this guided one experimental program.

5.2 Simulation of Navier-Stokes equation for 50 micron core microchannel reactor

For theoretical validation of the dye experiment, Simulation of Navier-Stokes equation was done to find out flow patterns and operating flow rate rate ratios of inner to outer region. Grid used for simulation is shown in figure *A*.10 of appendix A.

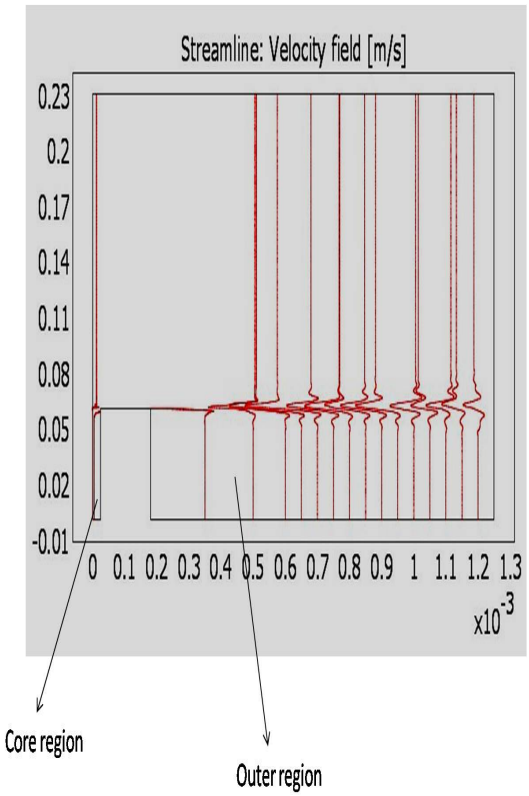

Figure 5.5: Stream line contours for inner to outer flow rate ratio 1:12

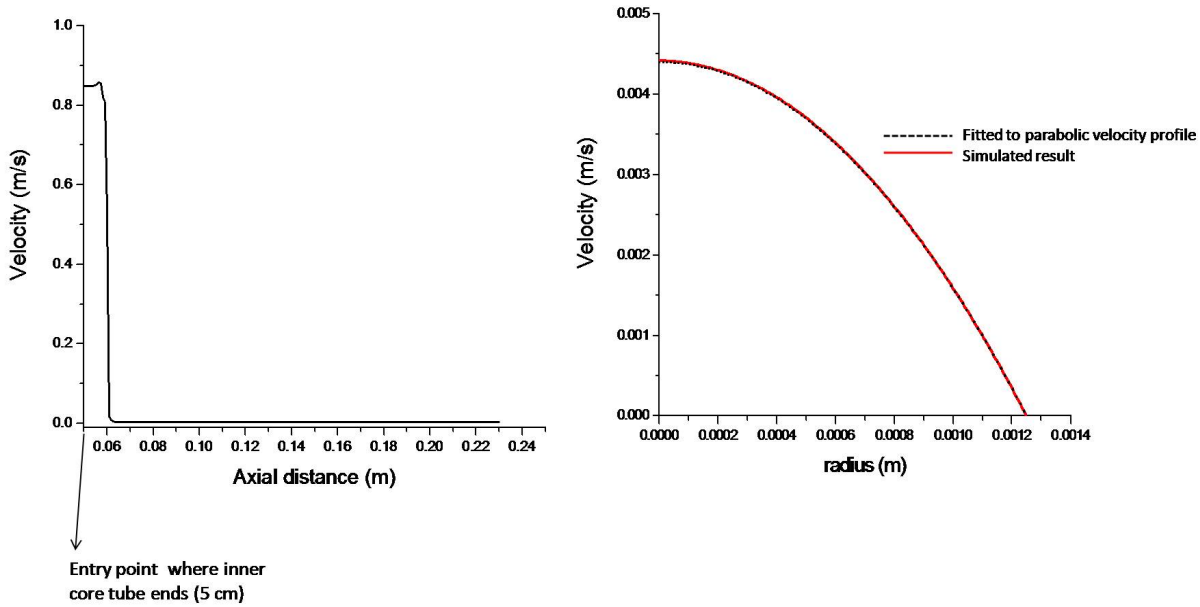

Figure 5.6: (A) Velocity profile at the center (r=0) as a function of axial distance and (B) Velocity profile at the exit of the reactor

Simulation results clearly suggest that outer region flow rate should be higher as compared to core region flow rate (figure 5.5). Figure 5.6 shows that velocity at center (r=0) became constant after 2 cm from the entrance. At the exit, the velocity profile is parabolic.

Chapter 6

Results and discussion

After visualizing the flow patterns with dye experiments in 50 micron core flow microchannel reactor (figure 4.6), experiments were carried out with gold salt solution and tannic acid to synthesize gold nanoparticles. Tannic acid acts as the reducing agent and stabilizing agent. Chloroauric acid was fed in the core at a flow rate 3 mL/hr and tannic acid was fed in the outer region at a flow rate 36 mL/hr. Syringe pumps were used to pump the liquids. Figure 6.1 shows the experimental setup.

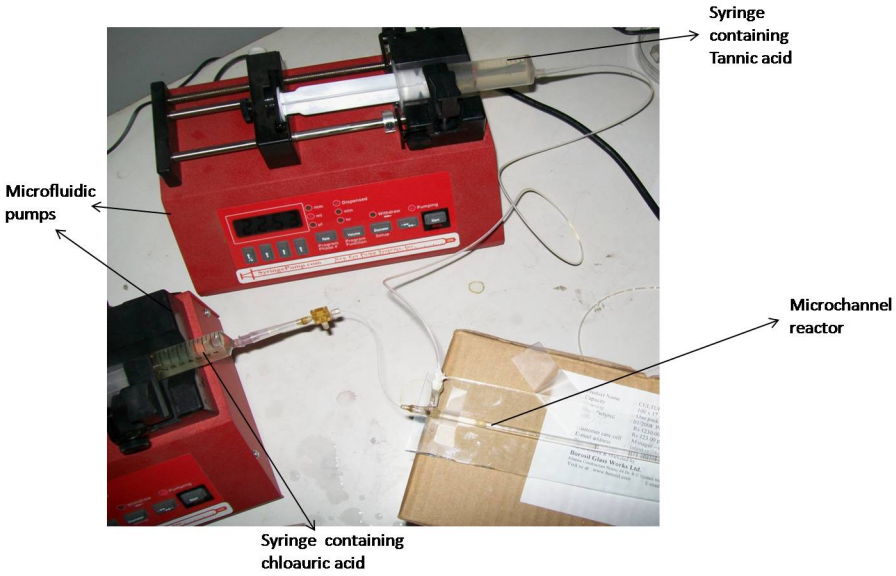

Figure 6.1: Digital micrograph of experimental setup

Samples were collected in deionized water stirred with magnetic stirrer continuously. The idea was to disperse the particles in water to avoid coagulation (figure 6.2).

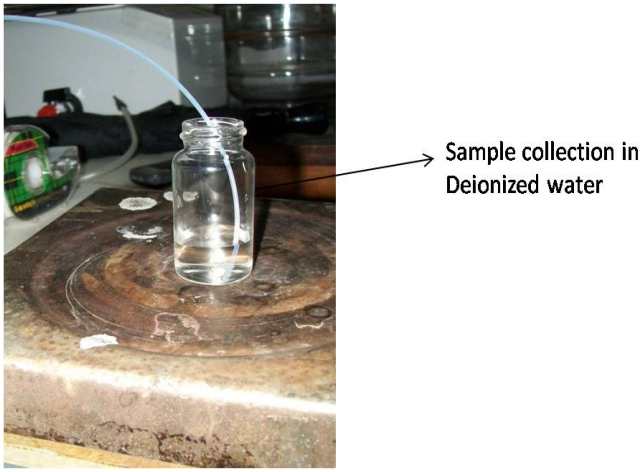

Figure 6.2: Digital micrograph of sample collection in deionized water at the outlet of microchannel

6.1 Experiments with 50 micron core flow microchannel reactor

In these experiments chloroauric acid concentration was 0.0017 M and tannic acid concentration was 0.0006 M. Figure 6.3 shows the UV-Visible spectra of samples collected from 50 micron core flow microchannel reactor from three trails. Run 1 and 2 have similar behavior. Run 3 shows little hump from 480 nm to 580 nm. The different values of absorbance can be attributed to different dilution factors in different runs. Bottommost curve (Run 3 with tannic acid background subtraction) presents the absorbance and wavelength curve with tannic acid as background subtraction. For this, tannic acid, used in the experiment, was placed in the reference cell of UV-Visible spectrometry. The variation in run 3 is attributed to the presence of an "unquantified" leak through the inlet connections

of syringe pumps. The absence of a characteristic surface plasmon resonance peak (expected around 520 nm for particles > 2nm) indicates that the gold is either in the form of nanoparticles with diameter < 2 nm or that gold is not completely reduced (which is unlikely given the long time duration between mixing and characterization). Unfortunately, TEM imaging using Tecnai T20 were inconclusive due to limits on resolution. In a few places, some larger sized particles (figure 6.4) were visualized, but these are not statistically representative of the sample.

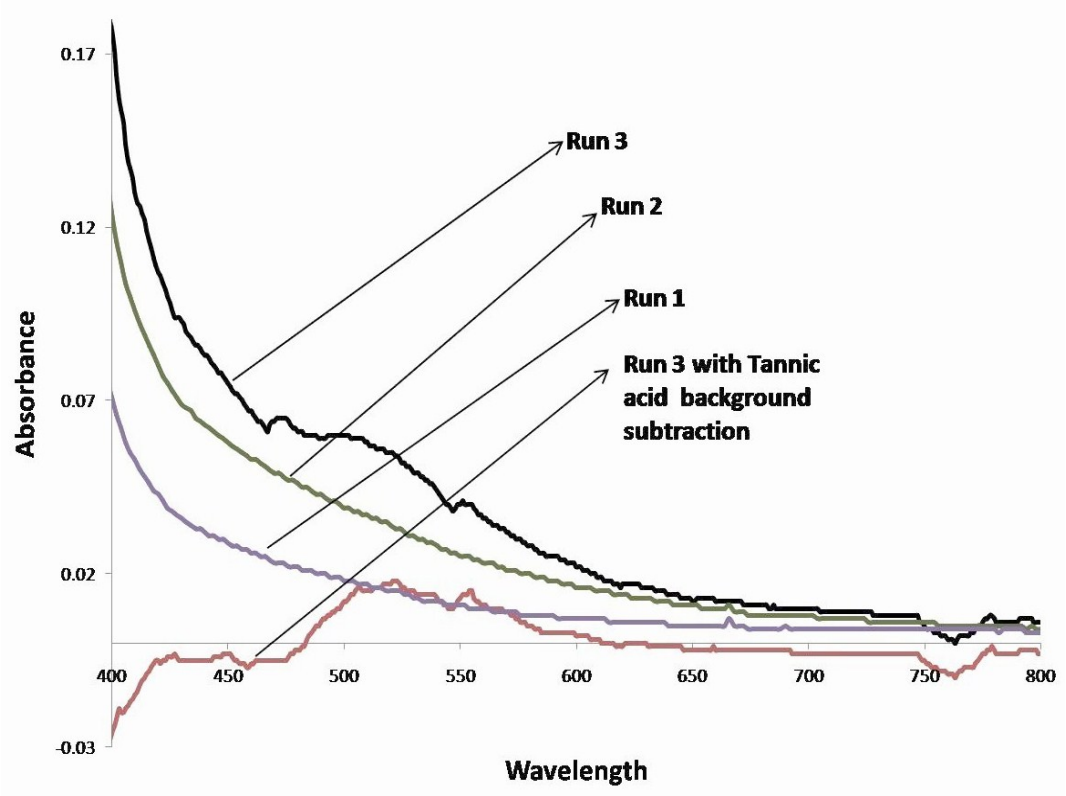

Figure 6.3: UV-visible spectra of gold nanoparticles synthesized in 50 micron core microchannel reactor core flow rate 3 mL/hr and outer flow rate 36 mL/hr

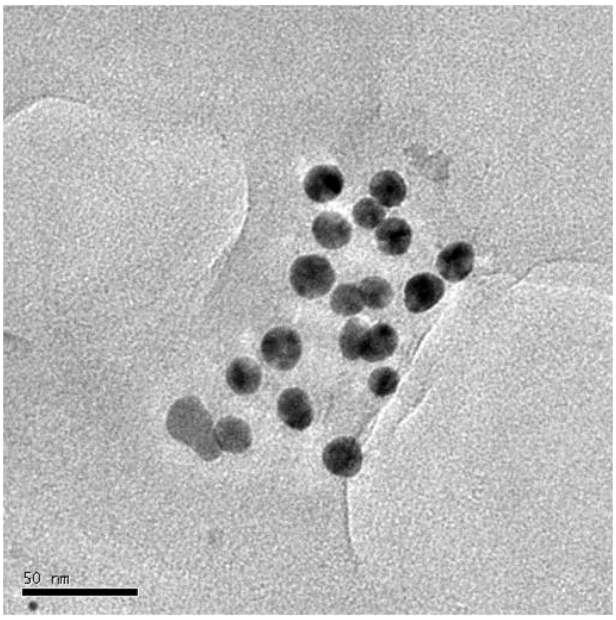

Figure 6.4: Sample TEM images of some large size gold nanoparticles (Scale bar: 50 nm)

6.1.1 Confirmation of gold presence

To confirm the presence of gold nanoparticles in the solution, one experiment was performed. A known amount of gold salt solution was added into tannic acid or a mixture of tannic acid and seeds (sample collected from 50 micron core flow microchannel reactor) by drop wise addition and mixed using a four blade Rushton turbine set up. A difference in UV-Visible peaks (figure 6.5) clearly indicates the presence of gold nanoparticles/precursors in the solution. Size analysis of the SEM images (performed after phase transferring to organic medium by thiol capping) of two samples also indicated a difference. Particle size is larger in the experiment using mixture of tannic acid and seeds (5.2 ± 2.1 nm) as compared to experiment having only tannic acid (4.3 ± 0.9 nm) (figure 6.6).

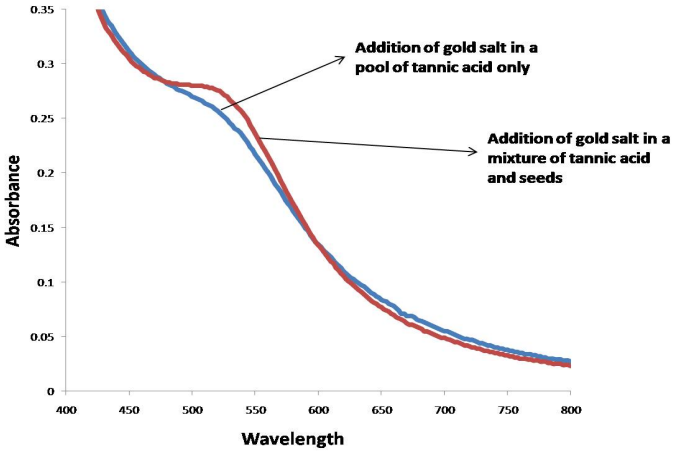

Figure 6.5: UV-visible spectra of gold nanoparticles synthesized by drop wise addition of gold salt solution in a pool of tannic acid or a mixture of tannic acid and seeds (Sample collected from 50 micron core flow microchannel)

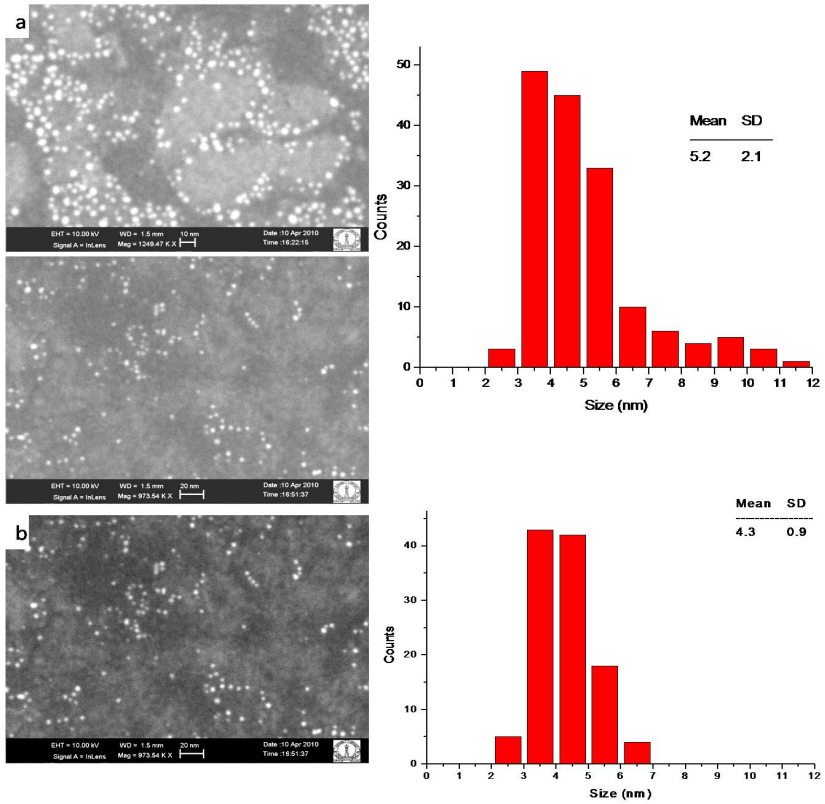

Figure 6.6: Representative SEM images (scale bar: 20 nm) and histograms for gold nanoparticles synthesized by drop wise addition: (a) in a mixture of tannic acid and seeds (b) in a pool of tannic acid only

6.1.2 Stability of the sample from 50 micron core flow microchannel reactor

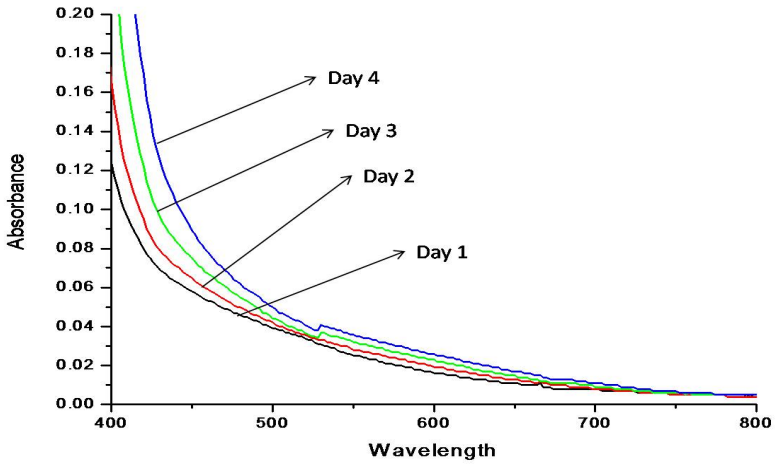

Figure 6.7: Comparison of UV-visible spectra of gold nanoparticles synthesized in 50 micron core microchannel reactor core flow rate 3 mL/hr and outer flow rate 36 mL/hr after different period of storage

Figure 6.7 shows UV-Visible spectrums of one sample collected from microchannel reactor on four successive days. All the curves are same and the deviation in the curves can be attributed to polymerization of tannic acid with time. It also shows that gold is in the form of particles of size $<$ 1-2 nm.

6.1.3 Comparison with batch systems

Two batch experiments were done. In one, gold salt solution was added to tannic acid at a constant flow rate of 3 mL/hr using 50 micron inner diameter PEEK tube, while in another experiment gold salt solution was added to tannic acid using micropipette in one shot. The total amount of gold salt solution added was kept constant which was equal to gold solution pumped in microchannel

experiment.

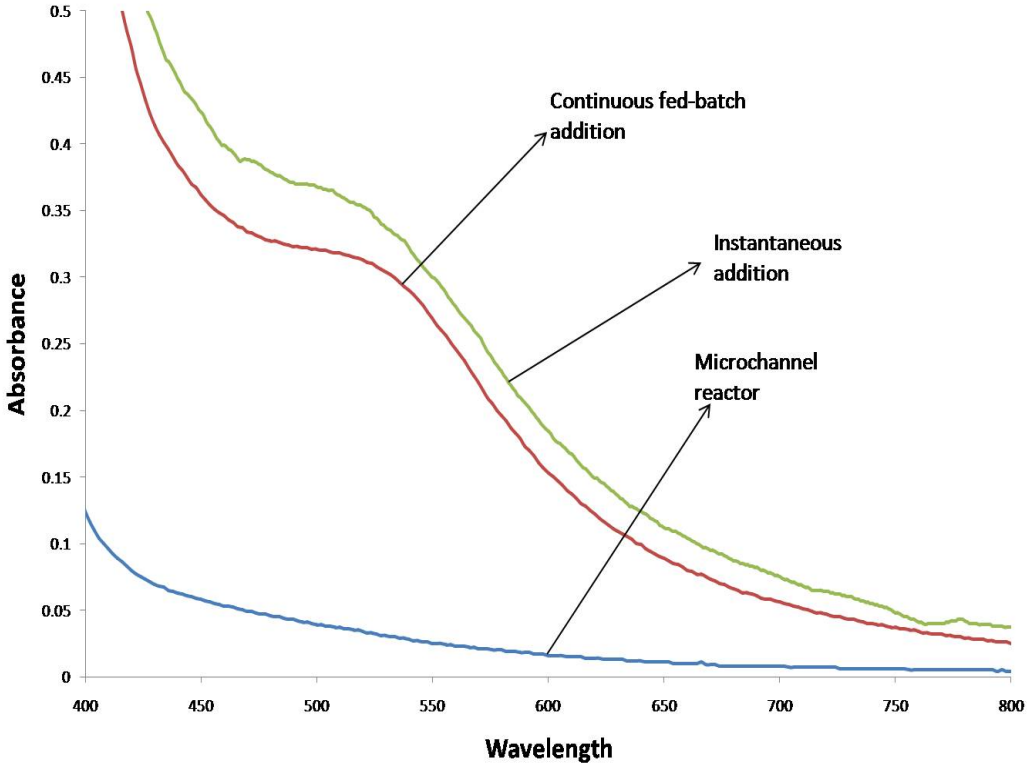

Figure 6.8: Comparison of UV-visible spectra of gold nanoparticles synthesized in 50 micron core microchannel reactor core flow rate 3 mL/hr and outer flow rate 36 mL/hr; continuous addition of god salt solution to tannic acid using 50 micron inner diameter PEEK tube and addition of gold salt solution to tannic acid using micropipette in a single shot

Figure 6.8 shows the UV-Visible spectra of two batch systems along with sample collected from microchannel reactor. Batch systems clearly have large size particles as compare to continuous system. In between batch systems, instantaneous addition has larger size (5.5 ± 1.2 nm) as compared to continuous fed-batch addition (3.0 ± 0.7 nm) (figure 6.9), while the C.V. is similar.

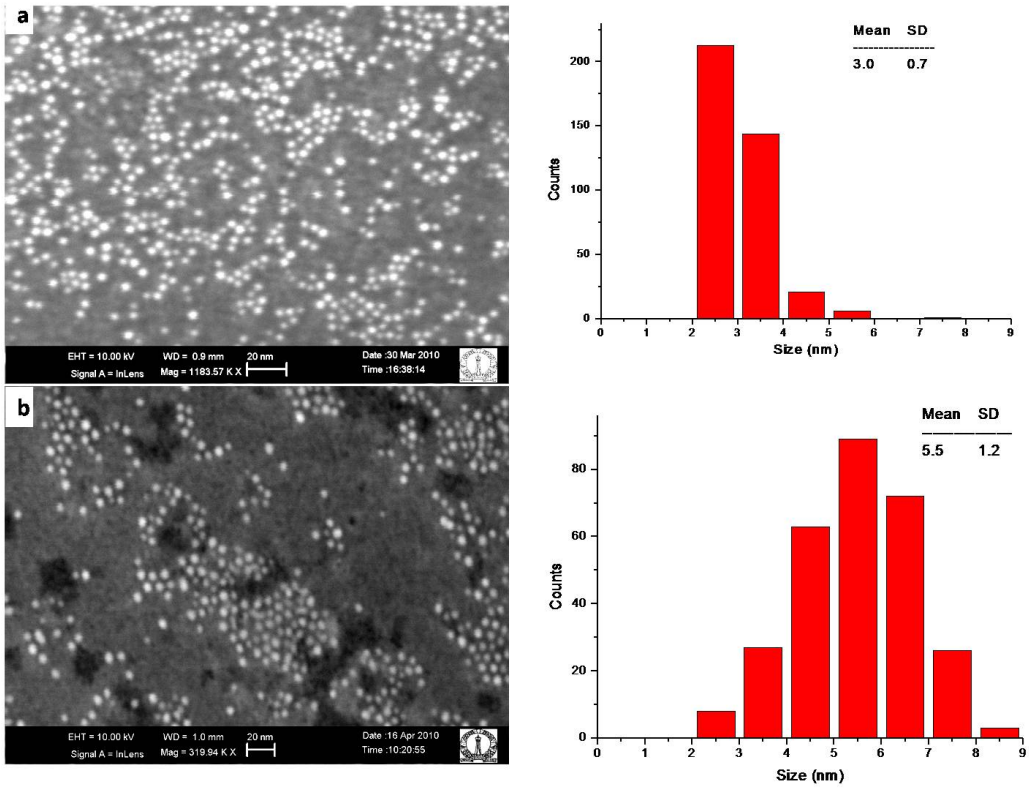

Figure 6.9: Representative SEM images and their size analysis (scale bar: 20 nm) for addition of gold salt solution to tannic acid: (a) continuously using 50 micron inner diameter PEEK tube (b) tannic acid using micropipette in single shot

6.1.4 Growth experiments

Sample collected from microchannel reactor was used as seeds for two different growth experiments a and b. Seeds formed in microchannel reactor were grown to bigger size by drop wise addition of gold salt solution and using Rushton turbine set up for mixing. In each growth experiment, addition of gold salt solution was done in two subsequent steps. In first step, gold salt solution was added to a mixture of seeds (synthesized in mcrochannel reactor) and tannic acid while in second step, particles synthesized in the first step act as seeds and gold solution was added to them .

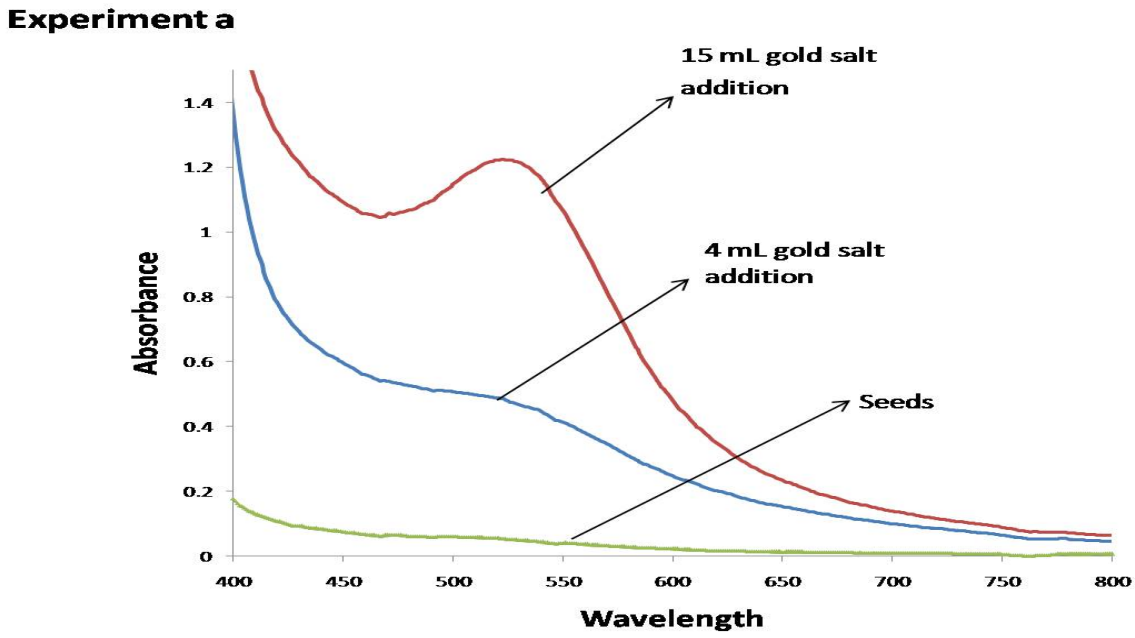

Figure 6.10: UV-visible spectra of gold nanoparticles synthesized in 50 micron core microchannel reactor with core flow rate 3 mL/hr and outer flow rate 36 mL/hr and for two subsequent steps of growth experiment a

Figure 6.10 represents the UV-Visible spectra for experiment a, where in first step 4 mL of gold solution was added and in second step 15 mL of the same

was added. The increase in absorbance of plasmon peak with gold salt addition indicates a increase in the amount of gold present in particle form.

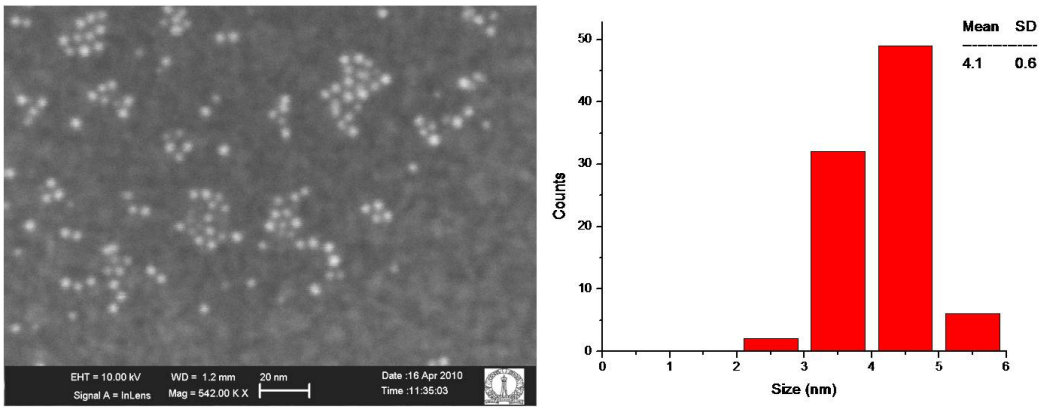

Figure 6.11: Representative SEM image (scale bar: 20 nm) and histogram for gold nanoparticles synthesized by addition of 4 mL of gold salt solution into a mixture of seeds (synthesized in microchannel reactor) and tannic acid

Figures 6.11 represents the SEM images and size distribution for first step of experiment a. Mean size of the particles was 4.1 ± 0.6 nm. Sample colour also changed from colourless to reddish (figure 6.13). In second step of experiment a, particle size increased from 4.1 ± 0.6 nm to 7.4 ± 1.1 nm (figure 6.12). Sample colour changed from reddish to deep red (figure 6.13).

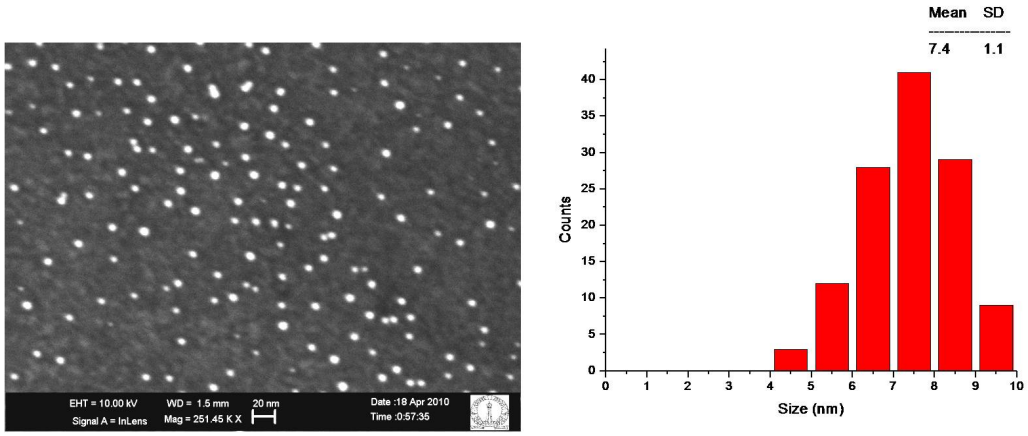

Figure 6.12: Representative SEM image (scale bar 20 nm) and histogram for gold nanoparticles synthesized in second step of experiment a

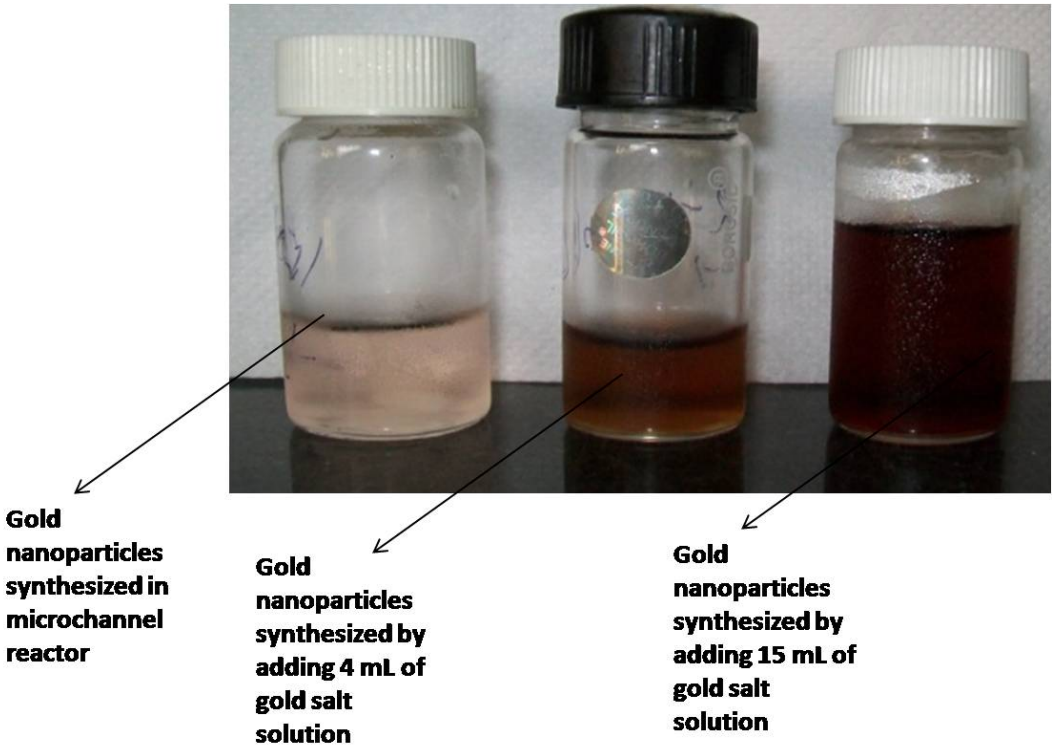

Figure 6.13: Digital micrograph of samples collected during growth experiment done by adding 4 mL and 15 mL of gold salt solution in subsequent steps of experiment a

A similar trend was observed in the experiment b as shown in UV-Visible spectra (figure 6.14), where size grows from 4.3 ± 0.8 nm (figure 6.15) in first step to 6.9 ± 1.6 nm (figure 6.16) in second step.

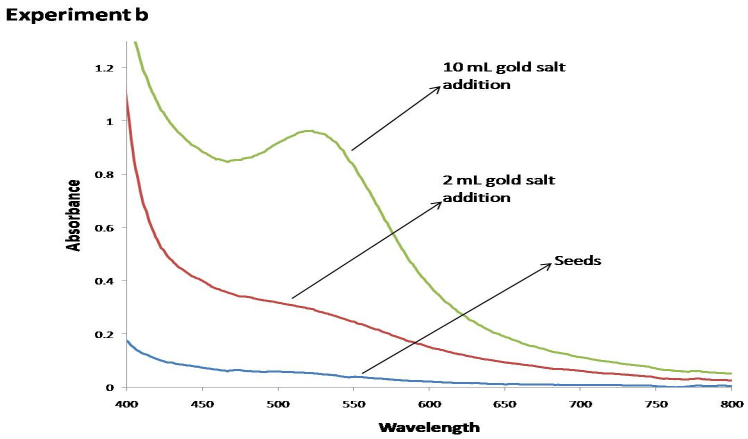

Figure 6.14: UV-visible spectra of gold nanoparticles synthesized in 50 micron core microchannel reactor with core flow rate 3 mL/hr and outer flow rate 36 mL/hr and for two subsequent steps of growth experiment b

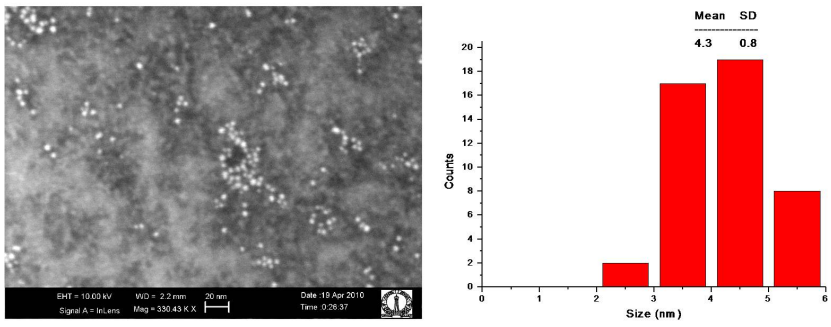

Figure 6.15: Representative SEM image (scale bar: 20 nm) and histogram for gold nanoparticles synthesized by addition of 2 mL of gold salt solution into a mixture of seeds (synthesized in microchannel reactor) and tannic acid

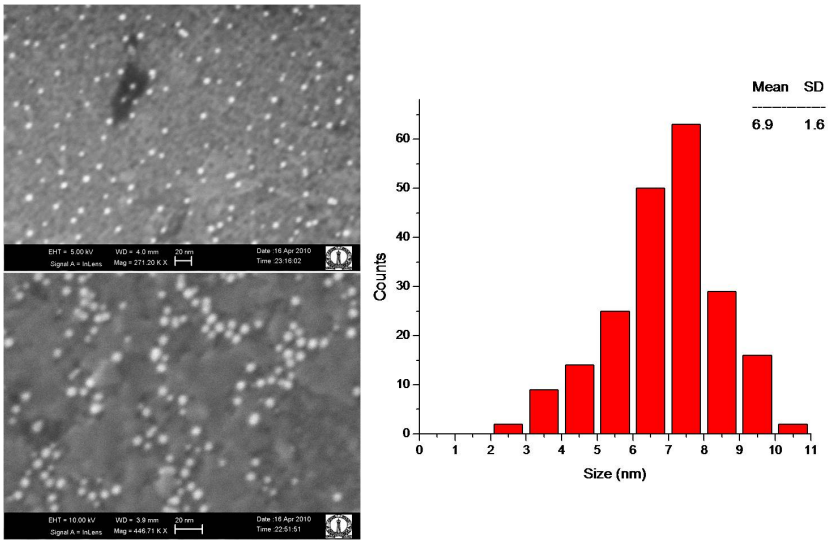

Figure 6.16: Representative SEM image (scale bar: 20 nm) and histogram for gold nanoparticles synthesized in second step of experiment b

Mass balance calculations were done to find out the mean size of seeds synthesized in microchannel reactor with the following assumptions.

1. All the seeds are of uniform size.
2. Growth is surface reaction controlled.
3. Gold atoms deposits on seeds uniformly.
4. There is no secondary nucleation and growth; only seeded growth takes place.

For experiment a

Table 6.1: Comparison of experimental mean size with theoretical mean size calculated using mass balance for growth experiment a

steps	theoretical size assuming initial seed size 1 nm	theoretical size assuming initial seed size 2 nm	Experimental size in nm
4 mL addition of gold salt solution	2.0	3.9	4.1 ± 0.6
15 mL addition of gold salt solution	3.8	7.5	7.4 ± 1.1

For experiment b

Table 6.2: Comparison of experimental mean size with theoretical mean size calculated using mass balance for growth experiment b

steps	theoretical size assuming initial seed size 1 nm	theoretical size assuming initial seed size 2 nm	Experimental size in nm
2 mL addition of gold salt solution	1.6	3.2	4.3 ± 0.8
10 mL addition of gold salt solution	3.5	6.7	6.9 ± 1.6

From mass balance calculations it looks like the seed size is close to 2 nm. If that would be case then particles should be visible in TEM. So, it can be concluded that particle size is less than 2 nm and along with seeded growth, secondary nucleation also takes place.

6.2 Effect of gold salt concentration

To find out the effect of gold salt concentration on particle size, gold salt concentration was increased 5 times keeping tannic acid concentration constant. Figure 6.17 shows the UV-Visible spectra of sample collected from microchannel reactor

and tannic acid. The difference between two curves indicates the consumption of tannic acid during the reaction in microchannel reactor.

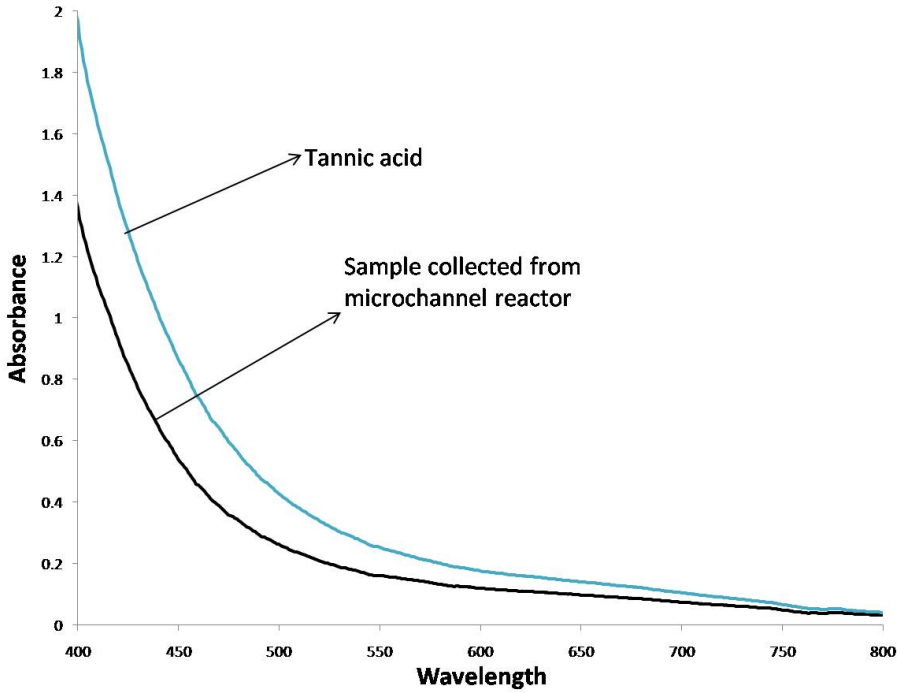

Figure 6.17: UV-Visible spectra of gold nanoparticles synthesized with gold salt concentration in 50 micron core microchannel reactor with core flow rate 3 mL/hr and outer flow rate 36 mL/hr

Figure 6.18 shows the TEM image of sample collected from the reactor. Lattice fringes with spacing of 0.29 nm were visible which corresponds to [110] planes of cubic gold lattice. Although the size of these domains in plane is > 5 nm, their thickness is on atomic scale. Hence, we couldn't detect the presence of these plates using UV-Vis spectroscopy as their surface plasmon resonance is known to occur in the near Infrared region (Fan *et al.*, 2010).

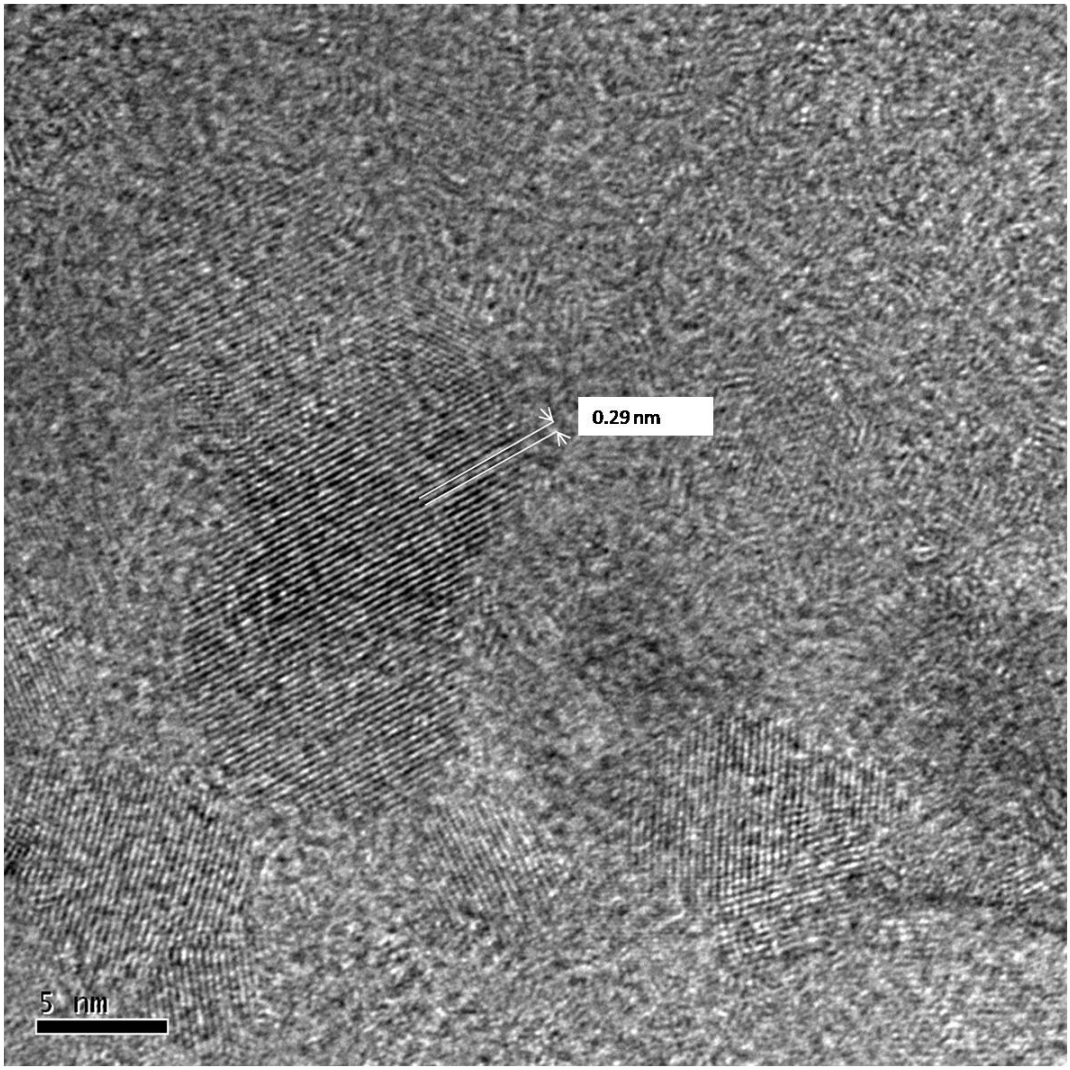

Figure 6.18: Representative TEM images of sample collected from microchannel reactor with gold salt concentration 0.0085 M with core flow rate 3 mL/hr and 36 mL/hr (scale bar: 5 nm)

6.2.1 Confirmation of presence of gold

For further confirmation of presence of gold, 8 mL of ethanol was added to 6 mL of sample in a test tube and left for 20 hours. After that solution was centrifuged at 3800 r.p.m. for 40 minutes. A red colour was obtained at the bottom of test tube. Presence of red colour can be attributed to agglomeration of nanoparticles, thereby conforming the presence of gold nanoparticles (figure 6.19).

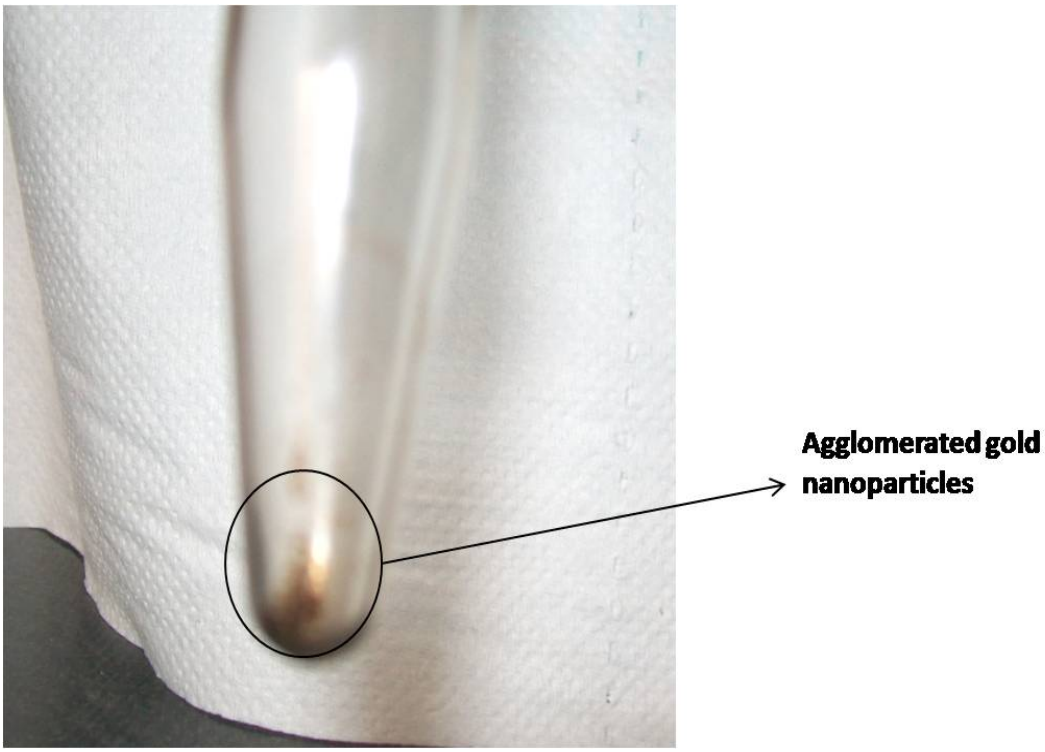

Figure 6.19: Digital micrograph of gold nanoparticles agglomerated and collected by centrifuging at the bottom of test tube

Atomic absorption spectra also gave a signal corresponding to presence of gold atoms. However, quantification is not possible at the moment. All these experiments confirm the reduction of gold salt and formation of gold nanostructures.

6.2.2 Catalytic activity

Carregal-Romero *et al.* (2010) showed that gold nanoparticles affect the rate of reduction of hexacynoferrate (III) by sodium borohydride in aqueous phase. Hexacynoferrate has peak at 420 nm in visible range. To check the catalytic activity of gold nanoparticles, two experiments were done. One was without gold nanoparticles and another one was with gold nanoparticles synthesized via microchannel reactor.

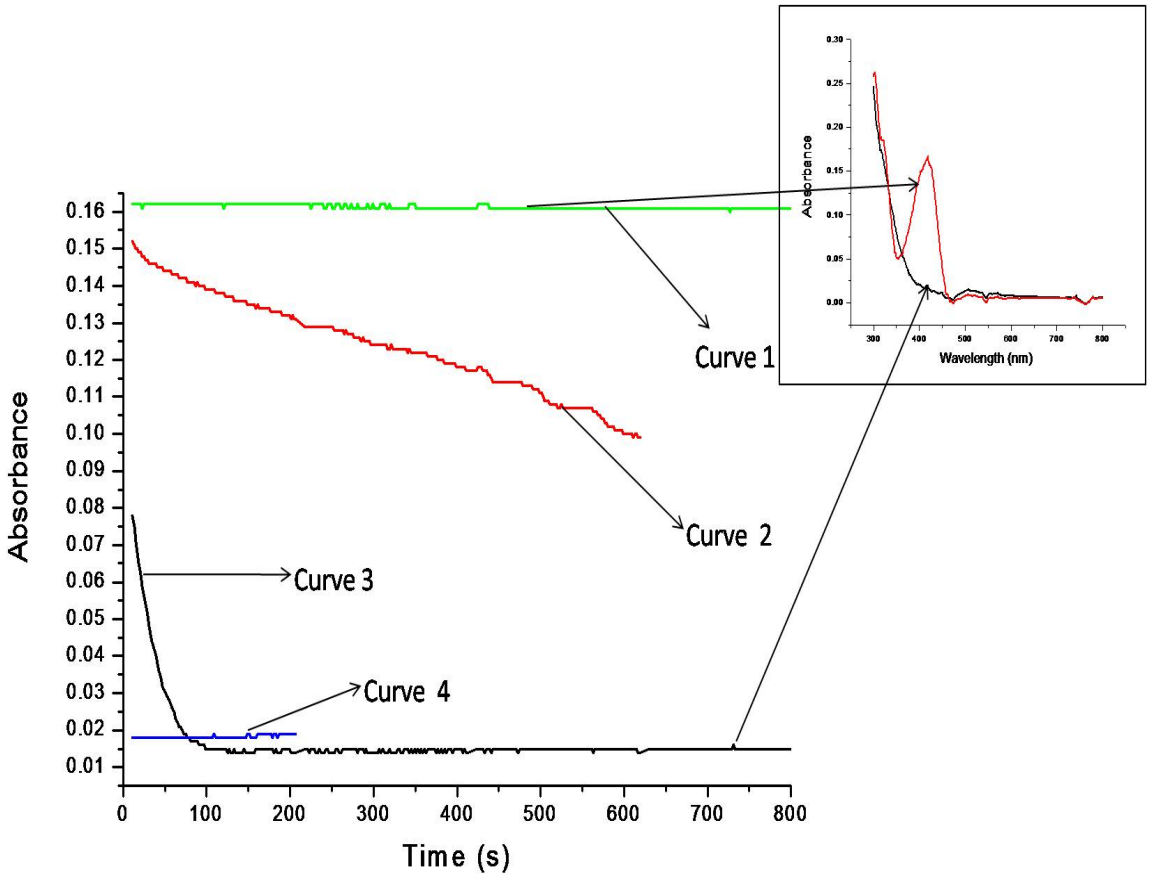

Figure 6.20: Absorbance and time spectra at 420 nm for (1) pure potassium hexacynoferrate (III) (2) potassium hexacynoferrate (III) on addition of sodium borohydride (3) a mixture of hexacynoferrate (III) and gold nanoparticles on addition of sodium borohydride (4) pure sodium borohydride

Figure 6.20 shows the absorbance vs. time plot at 420 nm wavelength. Curve 1 represents the absorbance of pure potassium hexacynoferrate (III). Absorbance remains constant with the time which shows that hexacynoferrate (III) is not degrading itself. Curve 2 shows the absorbance of mixture of potassium hexacynoferrate (III) and sodium borohydride. A decrease in absorbance shows the degradation of hexacynoferrate (III). Curve 3 shows the absorbance of a mixture of potassium hexacynoferrate (III), borohydride and gold nanoparticles. In presence of gold nanostructures, decrease in absorbance is much faster as compared to the absence of nanostructures. Curve 4 shows the absorbance of pure sodium borohydride. The inset shows the spectra of solutions used to determine curve 1 and used to determine curve 4 at time t = 810 s. Absence of peak at 420 nm indicates the complete reduction of potassium hexacynoferrate (III).

6.3 Experiments with 100 micron core flow microchannel reactor

Experiment was carried out with gold salt solution and tannic acid to synthesize gold nanoparticles in 100 micron core flow microchannel reactor. Chloroauric acid flows to the core side with a rate of 3 mL/hr and tannic acid flows to outer side at a rate of 36 mL/hr. Syringe pumps were used to pump the liquids (figure 6.1). The sample was collected in deionized water with continuous stirring by magnetic stirrer. Along with microchannel reactor experiment, a batch experiment was also done, in which gold salt was added in continuous manner to a pool of tannic acid using 100 micron inner diameter PEEK tube. Amount of gold added in batch experiment was equal to the amount pumped in microchannel experiment.

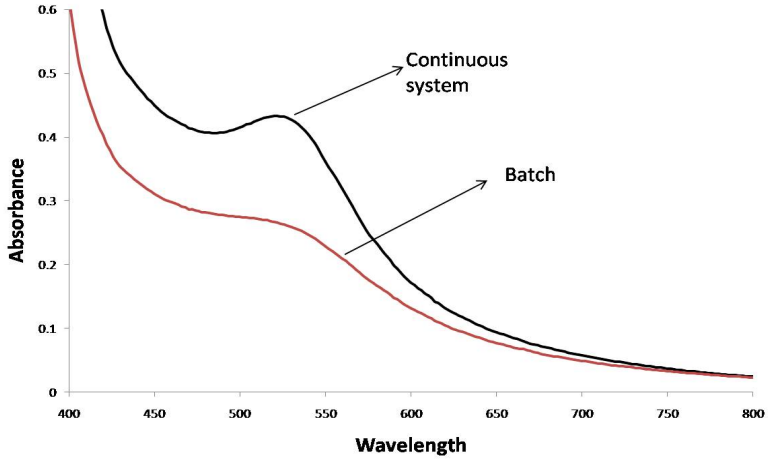

Figure 6.21: UV-visible spectra of gold nanoparticles synthesized in 100 micron core flow microchannel reactor with core flow rate of 3 mL/hr and outer flow rate of 36 mL/hr and continuous addition of gold salt solution to tannic acid using 100 micron inner diameter PEEK tube

Figure 6.21 represents the UV-Visible spectra of continuous as well as batch system. Difference in surface plasmon peak indicates the large size particles for continuous system as compare to batch system. SEM images have also confirmed the same. Continuous system has larger size particles (4.1 ± 1.5 nm) as compare to batch system (2.9 ± 0.7 nm) (figure 6.22). In this case, it appears, that the size of nanoparticles synthesized in microchannel is larger, in contrast to the findings using 50 micron core flow microchannel reactor. This aspect needs to be probed in detail in future experiments.

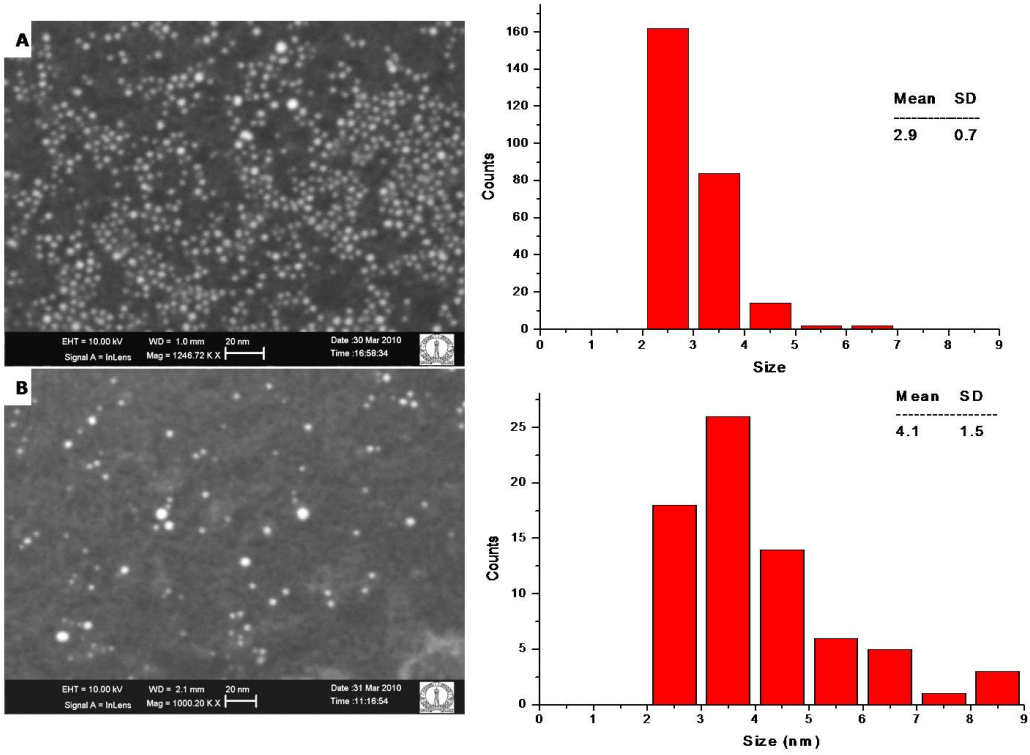

Figure 6.22: Representative SEM image (scale bar: 20 nm) and histogram for gold nanoparticles synthesized (A) Batch system (B) 100 micron core flow microchannel reactor

Chapter 7

Conclusions and recommendations

7.1 Conclusions

Diffusion length scale plays important role in determining size and shape of gold nanostructures synthesized in microchannel reactor. At room temperature, gold nanostructures were synthesized in 50 micron core flow microchannel reactor which were different from corresponding batch systems. Nanostructures exhibited catalytic activity in reduction of hexacynoferrate (III).

7.2 Recommendations for future work

The immediate future work can be focused to find the effect of gold nanostructures on the rate of reduction of hexacynoferrate. There are various parameters like flow rate, molar ratio of precursors, presence of stabilizer, that affects the particle size and polydispersity. Future work can be focused on the study of these parameters on particle size, shape and polydispersity.

Microchannel reactor can also be fabricated using lithographic technique. Spiral microchannel of SU-8 and PDMS has been made in our lab using lithographic technique (Iniyan, 2009). The future work in this regard involves the making of input and output structures in these channels and to further modify

the SU-8 microchannel. After that, experiments can be carried out to synthesize nanoparticles.

References

Allémann, E., Leroux, J. C. and Gurny, R. (1998) Polymeric nano- and microparticles for the oral delivery of peptides and peptidomimetics. *Advanced Drug Delivery Reviews* **34**, 171 – 189.

Andreev, V. P., Koleshko, S. B., Holman, D. A., Scampavia, L. D. and Christian, G. D. (1999) Hydrodynamics and mass transfer of the coaxial jet mixer in flow injection analysis. *Analytical chemistry* **71**, 2199–2204.

Brust, M., Walker, M., Bethell, D., Schiffin, D. J. and Whyman, R. (1994) Synthesis of thiol-derivatised gold nanoparticles in a two-phase liquid-liquid system. *Journal of the Chemical Society, Chemical Communications* pp. 801–802.

Carregal-Romero, S., Pérez-Juste, J., Hervés, P., Liz-Marzán, L. and Mulvaney, P. (2010) Colloidal Gold-Catalyzed Reduction of Ferrocyanate (III) by Borohydride Ions: A Model System for Redox Catalysis. *Langmuir* **26**, 1271–1277.

Daniel, M. C. and Astruc, D. (2004) Gold nanoparticles: Assembly, supramolecular chemistry, quantum-size-related properties, and applications toward biology, catalysis, and nanotechnology. *Chemical Reviews* **104**, 293–346.

Dyke, M. V. (1988) *A album of fluid motion*. The Parabolic Press, Stanford (California), Department of Mechanical Engineering, Stanford University, Stanford, California.

Fan, X., Guo, Z. R., Hong, J. M., Zhang, Y., Zhang, J. N. and Gu, N. (2010) Size-controlled growth of colloidal gold nanoplates and their high-purity acquisition. *Nanotechnology* **21**, 1–7.

Guo, S. and Wang, E. (2007) Synthesis and electrochemical applications of gold nanoparticles. *Analytica Chimica Acta* **598**, 181 – 192.

Gutsch, A., Krmer, M., Michael, G., Mhlenweg, H., Pridhl, M. and Zimmermann, G. (2002) Gas-phase production of nanoparticles. *Kona* **20**, 24–37.

Haruta, M. (2002) Catalysis of gold nanoparticles deposited on metal oxides. *Cattech* **6**, 102–115.

Haus, J. W., Zhou, H. S., Takami, S., Hirasawa, M., Honma, I. and Komiyama, H. (1993) Enhanced optical properties of metal-coated nanoparticles. *Journal of Applied Physics* **73**, 1043–1048.

Hepel, M. (1998) The electrocatalytic oxidation of methanol at finely dispersed platinum nanoparticles in polypyrrole films. *Journal Electrochemical Society* **145**, 124–135.

Iniyan, S. E. (2009) Synthesis of nanoparticles in microchannel reactor, project report .

Jähnisch, K., Hessel, V., Löwe, H. and Baerns, M. (2004) Chemistry in microstructured reactors. *Angewandte Chemie International Edition* **43**, 406–446.

José-Yacamán, M., Mehl, R. and Medalist, A. (1998) The role of nanosized particles. A frontier in modern materials science, from nanoelectronics to environmental problems. *Metallurgical and Materials Transactions A* **29**, 713–725.

Kirner, T., Albert, J., Günther, M. and Köhler, J. M. (2004) Static micromixers for modular chip reactor arrangements in two-step reactions and photochemical activated processes. *Chemical Engineering Journal* **101**, 65–74.

Köhler, J. M., Wagner, J. and Albert, J. (2005) Formation of isolated and clustered Au nanoparticles in the presence of polyelectrolyte molecules using a flow-through Si chip reactor. *Journal of Materials Chemistry* **15**, 1924–1930.

Kruis, F. E., Fissan, H. and Peled, A. (1998) Synthesis of nanoparticles in the gas phase for electronic, optical and magnetic applications–a review. *Journal of Aerosol Science* **29**, 511–535.

Mantzaris, N. V. (2005) Liquid-phase synthesis of nanoparticles: Particle size distributiondynamics and control. *Chemical Engineering Science* **60**, 4749–4770.

Mijatovic, D., Eijkel, J. and Berg, A. (2005) Technologies for nanofluidic systems: top-down vs. bottom-up-a review. *Lab on a Chip* **5**, 492–500.

Rolland, J. P., Dam, R. M. V., Schorzman, D. A., Quake, S. R. and DeSimone, J. M. (2004) Solvent- resistant photocurable liquid teflon for microfluidic device fabrication. *Journal of American Chemical Society* **126**, 2322–2323.

Sankar, K., Santhanam, V. and Kumar, S. (Manuscript under review, 2010) Room temperature protocol for gold nanoparticle synthesis: size control by slow addition. *Gold Bulletin* .

Schmid, H. K., Aslan, M.and Assmann, S., Nasz, R. and Schmidt, H. (1998) Microstructural characterization of Al_2O_3-SiC nanocomposites. *Journal of the European Ceramic Society* **18**, 39–49.

Shalom, D., Wootton, R. C. R., Winkle, R. F., Cottam, B. F., Vilar, R., deMello, A. J. and Wilde, C. P. (2007) Synthesis of thiol functionalized gold nanoparti-

cles using a continuous flow microfluidic reactor. *Materials Letters* **61**, 1146–1150.

Shipway, A. N., Katz, E. and Willner, I. (2000) Nanoparticle arrays on surfaces for electronic, optical, and sensor applications. *Journal of Chemical Physics and Physical Chemistry* **1**, 18–52.

Slot, J. W. and Geuze, H. J. (1985) A new method of preparing gold probes for multiple-labeling cytochemistry. *European journal of cell biology* **38**, 87–93.

Tsunoyama, H., Ichikuni, N. and Tsukuda, T. T. (2008) Microfluidic Synthesis and Catalytic Application of PVP-Stabilized, 1 nm Gold Clusters. *Langmuir* **24**, 11327–11330.

Turkevich, J., Stevenson, P. C. and Hillier, J. (1951) A study of the nucleation and growth processes in the synthesis of colloidal gold. *Discussions of Faraday Society* **11**, 55–75.

Wagner, J., Kirner, T., Mayer, G., Albert, J. and Köhler, J. M. (2004) Generation of metal nanoparticles in a microchannel reactor. *Chemical Engineering Journal* **101**, 251–260.

Wagner, J. and Köhler, J. M. (2005) Continuous synthesis of gold nanoparticles in a microreactor. *Nano letters* **5**, 685–691.

Appendix A

A.1 Protocol for core flow microchannel reactor

Figure *A*.1 represents the schematic diagram of core flow microchannel reactor

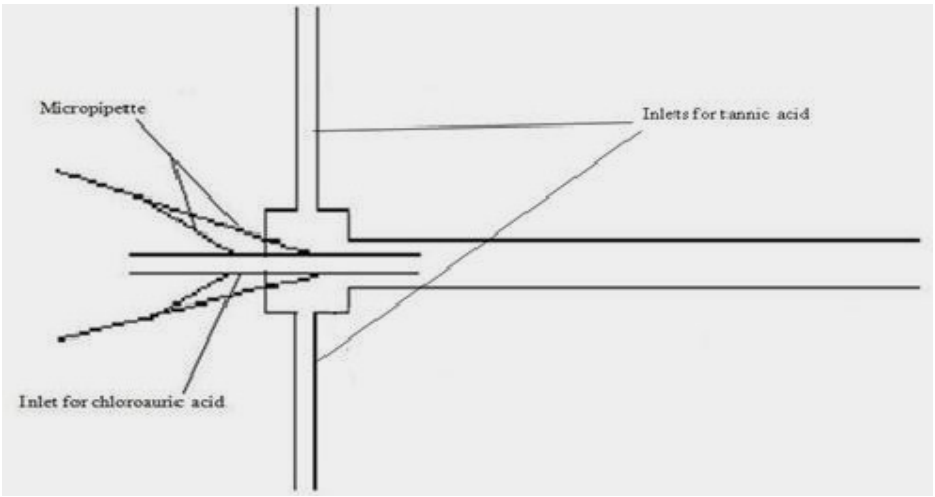

Figure A.1: Schematic diagram of core flow microchannel reator

A.1.1 Module for core flow PDMS microchannel reactor

A mould made up of glass pieces and a micropipette tip is shown in figure *A*.2.

Steps in making mould:

1. A glass tube having outer diameter of 6 mm (approximately) was taken. In one end of the tube a micropipette tip was fixed using Fevi-Kwik. At

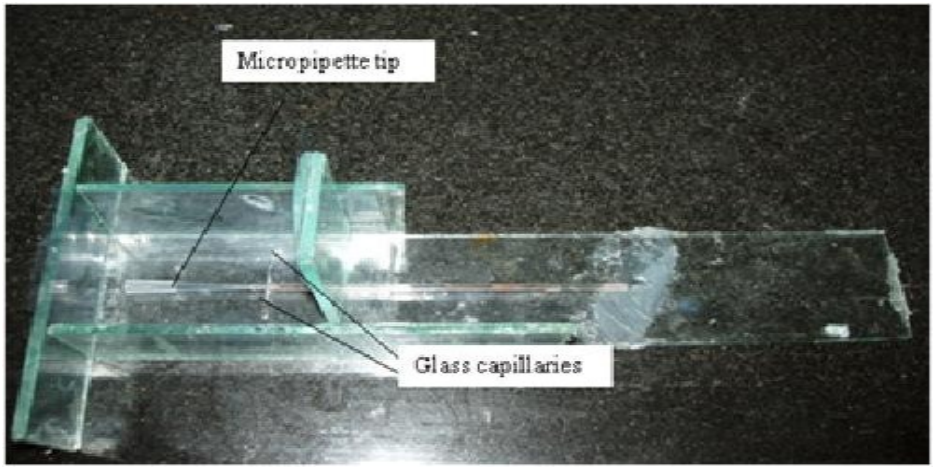

Figure A.2: Mould for core flow PDMS microchannel reactor

the sides of the tube two glass capillaries having outer diameter of 1.7mm and length of 3 cm (approximately) were attached using Fevi Kwik.

2. Glass tube structure made in 1st step joined with glass pieces other with the help of Fevi Kwik to get the shape shown in figure A2.

3. To fill all the gaps in the mould silicone was used.

4. After filling with silicone, mould was heated at 60 ^{0}C for 20 minutes in an oven.

5. Mould was taken out from the oven and water was poured in it to check the leakage.

A.1.2 Making of microchannel

PDMS base and curing agent were taken in the ratio 10:1 by weight in a petridish. Base and curing agent were mixed thoroughly by stirring the mixture manually for 15 minutes. Then the petridish containing PDMS mixture was put in a vacuum desiccator to remove air bubbles. After removing the air bubbles,

PDMS mixture was poured into the mould and allowed to rest for 20 minutes so that air bubble formed during pouring float out. Mould was heated at 60 ^{0}C for 2 hours in the oven and then taken out to cool down to room temperature. Glass structures were removed manually. After removing glass mould, PDMS structure was soaked in hexane to make it swell so that the internal capillaries and the micropipette tip can be removed. Then the PDMS structure was placed in ethanol medium so that it can shrink back to its original size. A micropipette tip containing a glass capillary of diameter around 500 microns was inserted in PDMS structure. To avoid the mixing of two liquids at the junction, glass capillary was properly sealed within the micropipette. Core flow PDMS microchannel reactor is shown in figure *A*.3.

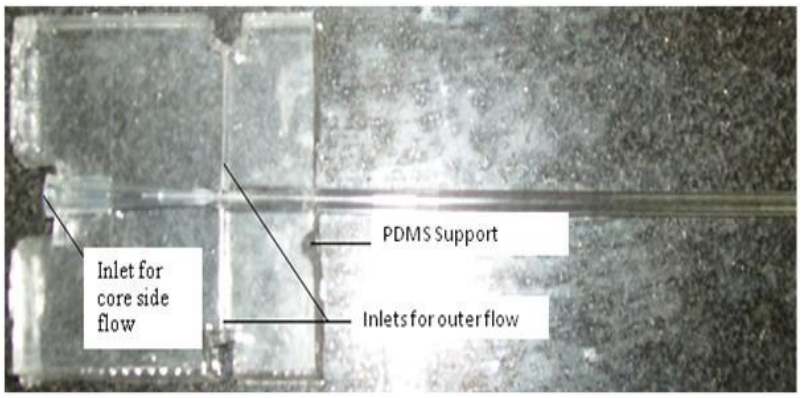

Figure A.3: Digital micrograph PDMS microchannel reactor

A.2 TEM data analysis for gold nanoparticles synthesized in core flow microchannel reactor

A.2.1 At core flow rate 20μ L/s

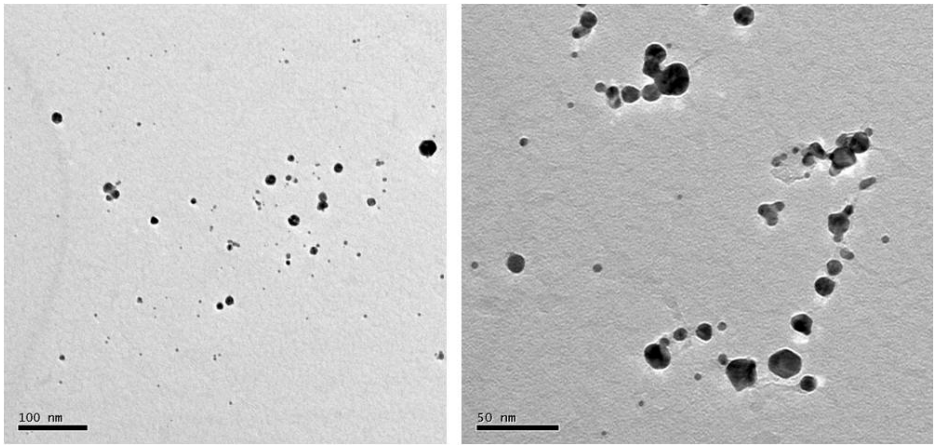

Figure A.4: TEM representative of gold nanoparticle synthesized in core flow microchannel reactor. Conditions: Chloauric acid (core side) at flow rate of 20 μL/s, tannic acid (outer side) at flow rate 12.6 times the core flow rate

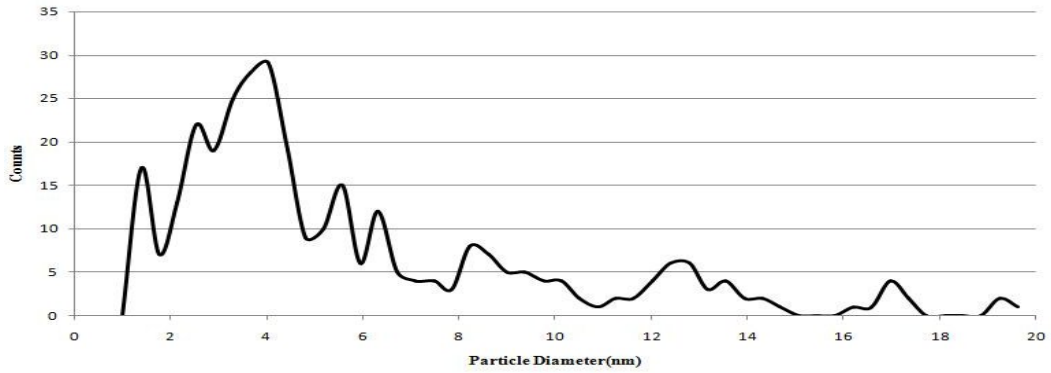

Figure A.5: Size distribution of gold nanoparticle synthesized in core flow microchannel reactor. Conditions: Chloauric acid (core side) at flow rate of 20 μL/s, tannic acid (outer side) at flow rate 12.6 times the core flow rate

A.2.2 At core flow rate 50μ L/s

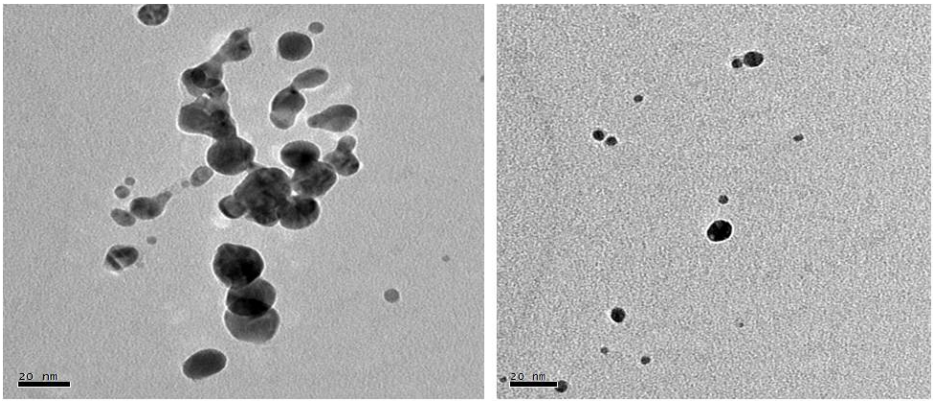

Figure A.6: TEM representative of gold nanoparticle synthesized in core flow microchannel reactor. Conditions: Chloauric acid (core side) at flow rate of 50 μL/s, tannic acid (outer side) at flow rate 12.6 times the core flow rate

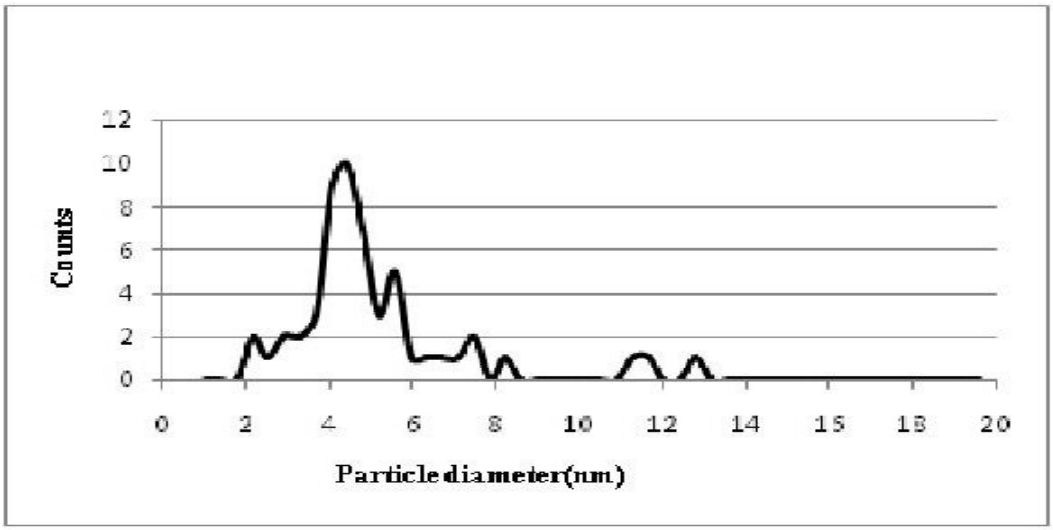

Figure A.7: Size distribution of gold nanoparticle synthesized in core flow microchannel reactor. Conditions: Chloauric acid (core side) at flow rate of 50 μL/s, tannic acid (outer side) at flow rate 12.6 times the core flow rate

A.3 Grids used for simulation

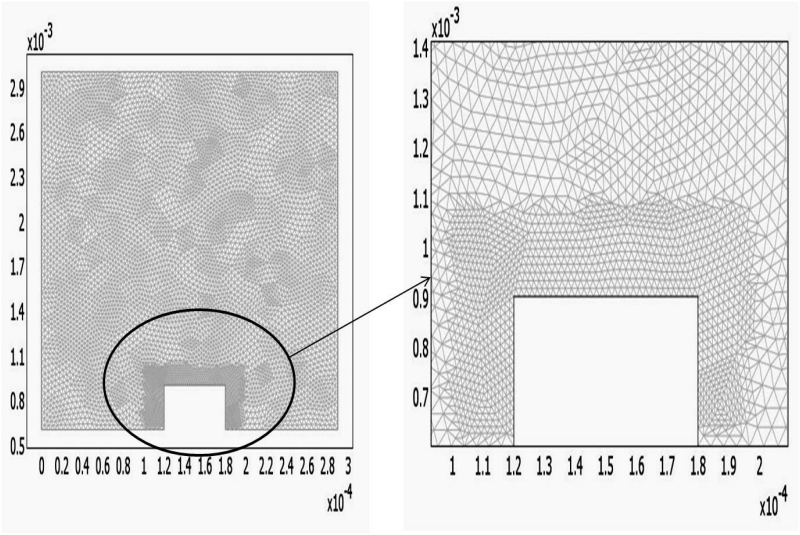

Figure A.8: Grid used for simulation of velocity stream line contours in core flow type geometry reported by Andreev *et al.* (1999)

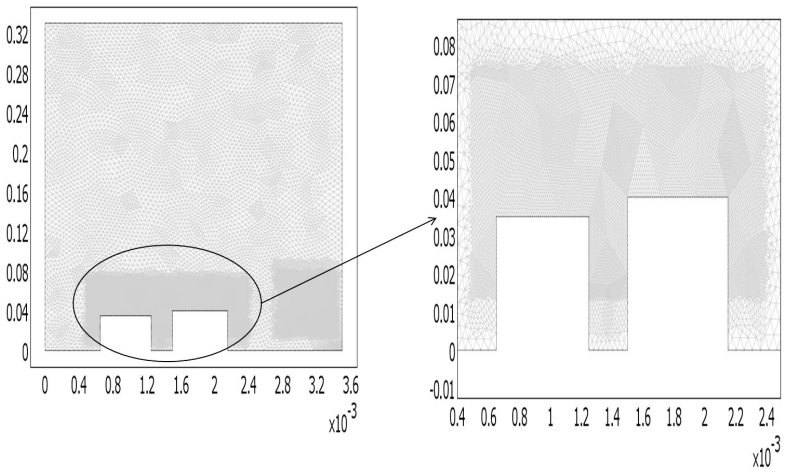

Figure A.9: Grid used for simulation of velocity stream line contours in 'core in core' flow type geometry

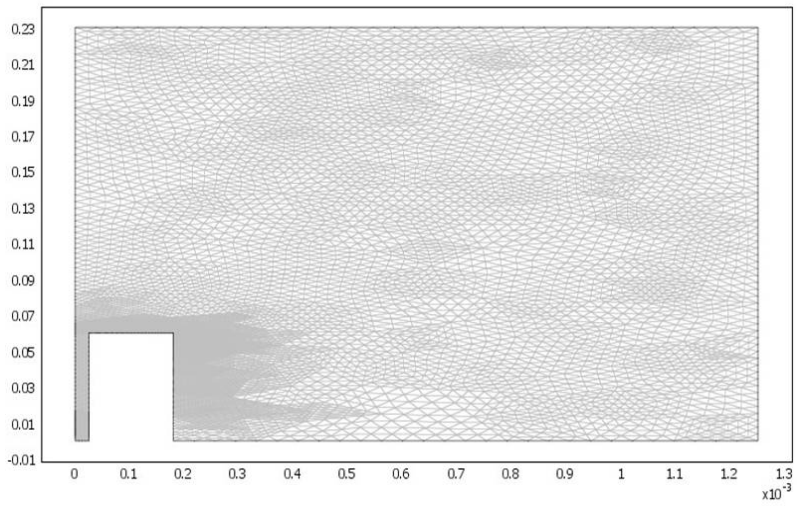

Figure A.10: Grid used for simulation of velocity stream line contours in 50 micron core flow microchannel reactor

A.4 List of chemicals used

- Gold (III) chloride hydrate, 99.999 % purchased from ALDRICH.
- Tannic acid, ACS reagent purchased from ACROS.
- Potassium carbonate, $\geq$ 98 % purchased from MERCK
- Sodium borohydride, 98 % purchased from ALDRICH
- Deionized water from Mili-Q water purification system of MILIPORE